KeA1

CHINESE ROOTS
GLOBAL IMPACT

Contents lists available at ScienceDirect

Petroleum Science

journal homepage: www.keaipublishing.com/en/journals/petroleum-science



Original Paper

Middle Eocene terrestrial paleoweathering and climate evolution in the midlatitude Bohai Bay Basin of eastern China



Di Chen ^{a, b}, Fu-Jie Jiang ^{a, b, *}, Xiong-Qi Pang ^{a, b}, Ling-Jian Meng ^c, Zheng-Jun Wang ^c, Zhi Xu ^{a, b}, Xue Zhang ^d, Li-Na Huo ^{a, b}, Jia-Hao Wen ^{a, b}, Ren-Jie Zhao ^{a, b}, Yuan Li ^{a, b}

- ^a State Key Laboratory of Petroleum Resources and Prospecting, Beijing, 102249, China
- ^b College of Geosciences, China University of Petroleum (Beijing), Beijing, 102249, China
- ^c PetroChina Jidong Oilfield Company, Tangshan, Hebei, 063004, China
- ^d Chinese Academy of Natural Resources Economics, Beijing, 100035, China

ARTICLE INFO

Article history: Received 11 September 2021 Received in revised form 17 October 2022 Accepted 29 December 2022 Available online 30 December 2022

Edited by Jie Hao and Teng Zhu

Keywords: Middle Eocene Paleoclimate Weathering MES shales Bohai Bay Basin

ABSTRACT

The middle Eocene climatic optimum (MECO, ca. ~42 Ma) is a key time period for understanding Cenozoic cooling of the global climate. Still, midlatitude terrestrial records of climate evolution during MECO epoch are rare. In this study, continuous high-resolution record of shale sediments in mid-Eocene Shahejie Formation (MES shales) in the Bohai Bay Basin were performed with major-element and wavelet analysis. The midlatitude paleoweathering and paleoclimatic evolution during MECO epoch were analyzed in this study. The MES shales experienced weak-moderate paleoweathering under a subtropical monsoon paleoclimate with mean annual temperature of 8.3-12.9 °C and mean annual precipitation of 685-1100 mm/yr. The MES shales record a mixed provenance involving intermediate igneous rocks, and low compositional maturity. The nutrient-rich environment led to enrichment in organic matter in the MES shales. Wavelet analysis revealed good periodicity about the paleoclimate and weathering during MECO epoch. In the stage I of MES shales depositional process, the paleolake was high in nutrients, and the MES shales experienced high chemical weathering due to a relatively warmer and more humid climate. In contrast, the climate in stage II was relatively cold and dry, and the maturity of the MES shales was relatively high during this stage, suggesting a relatively stable tectonic background. This work provides more terrestrial records of MECO epoch for midlatitude region, and is benefit for better understanding of the palaeoenvironment when MES shales formed. The implication of organic matters enrichment in this study is meaningful for the shale oil/gas exploration in Nanpu Sag.

© 2023 The Authors, Publishing services by Elsevier B.V. on behalf of KeAi Communications Co. Ltd. This is an open access article under the CC BY-NC-ND license (http://creativecommons.org/licenses/by-nc-nd/4.0/).

1. Introduction

The Eocene was a time of large shifts in the global environments following the disruption that occurred at the Paleocene-Eocene Thermal Maximum (PETM, 55.5 Ma; Zachos et al., 2001). Temperatures were generally warm, and the global climate is sometimes described as a period of "doubthouse" climate, transitional or intermediate between the greenhouse world of the Mesozoic through early Eocene, and the icehouse world of the Oligocene through to today (Miller et al., 1991; Zachos et al., 1993, 1994; Prothero, 2009;

E-mail address: jfjhtb@163.com (F.-J. Jiang).

Passchier et al., 2013, 2017). The polar regions were replete with sub-tropical fauna and flora (Prothero, 2009). Tropical proxies are known to suffer more from diagenetic alteration (Rohl et al., 2000). Evolutionary increases in diversity, and increasing productivity marked this epoch (Jahren et al., 2001). The magnitude and duration of carbon flux and climatic change across the PETM are typical record that may approximate the pace of industrial anthropogenic emissions (Bains et al., 1999). The future climate may be the recurrence of Eocene warm period with the increase of global greenhouse gas concentration. Thus, understanding the driving mechanism of Eocene climate and the fate of the carbon during this episode may lead to insights into the eventual of anthropogenic carbon

During Eocene, the middle Eocene climatic optimum (MECO, ca. ~42 Ma) is significant interval of transient warming event (Bohaty

 $[\]ast$ Corresponding author. State Key Laboratory of Petroleum Resources and Prospecting, Beijing, 102249, China.

D. Chen, F.-J. Jiang, X.-Q. Pang et al. Petroleum Science 20 (2023) 1471–1487

and Zachos, 2003; Kargaranbafghi and Neubauer, 2017). MECO is recorded worldwide by an excursion of ~1.0% benthic δ^{18} O records in fine-fraction suggesting 4 °C warming of both surface and intermediate deep waters, and pronounced changes in δ^{13} C values and coeval oscillations in the global carbonate compensation depth (Bohaty and Zachos, 2003; Bohaty et al., 2009). Its induced mechanism has been widely discussed, focusing Uplift of Oinghai Tibet Plateau, global sea level decline and the rise of monsoon climate etc. (Chung et al., 1998; Bohaty and Zachos, 2003; Ao et al., 2020). While, these predispositions have great differences and contradictions. The coupling relationship between the fine structure of geological records and the climate environment is still unclear. At present, most interpretations are based on marine sedimentary records, but the typical marine sediment thickness is about 1–2 m with low resolution, and it is vulnerable to biological disturbance. It is clear that the high resolution study of deep-time climate events is likely to be an increasingly fruitful line of research in understanding the earth system (Zachos and Dickens, 2000). The lacustrine sediments recorded more details about MECO with relatively high rate, but few relevant studies were reported at present.

Sedimentary record is strongly associated with the weathering of the lithosphere, which is affected directly by climate (McInerney and Wing, 2011). Weathering represents the interface and direct interaction between the lithosphere, atmosphere, hydrosphere and biosphere (Nesbitt and Young, 1982, 1989). The interaction between precipitation and mineral grains in a rock, and results in selective dissolution of soluble components: hydration: and consequently. formation of new minerals (Perri, 2018). The silicate weathering on land facilitates the preservation of carbonates, which is an important mechanisms of atmospheric CO₂ drawdown (Panchuk et al., 2008). The carbon released into the atmosphere during the PETM period can return to the pre-event level in 100 years only through weathering. Generally, weathering is generally enhanced under hot and humid conditions and suppressed under cold and dry conditions (Eberl et al., 1984; Perri and Ohta, 2014; Perri, 2018; Szymański and Szkaradek, 2018). The effects of weathering can be interpreted by analyzing the changes in the element compositions of a sediment profile (Nesbitt and Young, 1989; Perri et al., 2012, 2016). In addition to weathering conditions, the provenance (Armstrong-Altrin et al., 2013; Bakkiaraj et al., 2010; Cullers, 2000, 2002) and tectonic setting of a sedimentary basin (Armstrong-Altrin et al., 2013; Fatima and Khan, 2012) also have strong effects on the elemental compositions of clastic sediments. Hence, these factors must be interpreted collectively in order to disentangle their individual effects and mutual interactions.

To investigate continental weathering and paleoclimate changes at various temporal and spatial scales during MECO event, this study provides a continuous high resolution profile at the midlatitude East Asian continent. This profile focus on the middle Eocene lacustrine shale sediments at the Shaheije Formation of Bohai Bay Basin, which offers a well-preserved in-situ core sedimentary record under MECO event (42-42.5 Ma; Chen et al., 2019). The elemental composition of sediments in 50 m interval in core well A1 was measured at 1m intervals with X-ray fluorescence (XRF) method. It allows high-resolution, nearly continuous, nondestructive analyses of major and minor elements at the fresh surfaces. Spectral analysis is used to analyze the periodicity of paleoenvironmental changes under paleontological age constraint. The aims of this study are to 1) provide more details about the lacustrine records of MECO event; 2) reconstruct the history of paleoclimate and paleoweathering of the mid-latitude East Asian continent during middle Eocene; and 3) to provide more information on the role of midlatitude physical and biogeochemical processes in the global climate system during the middle Eocene.

2. Geological setting

The Mesozoic-Cenozoic Bohai Bay Basin, located in northeastern China, is a typical midlatitude rift basin (34°N-42°N; Fig. 1; Allen et al., 1997; Dong et al., 2010). It experienced regional extension along with widespread faulting in response to subduction roll-back at the active convergent Asian-Pacific plate boundary during Eocene period (Allen et al., 1997). Due to the regional tectonics in the early Tertiary, regional extension occurred in conjunction with weak convergence and formed numerous secondary structural units with Paleogene rifts in the Bohai Bay Basin (Fig. 1; Allen et al., 1997; Dong et al., 2010). The basin was filled by a thick terrestrial clastic succession resting on pre-Cenozoic basement. In the Eocene, abundant organic-rich lacustrine mudstones and shales were deposited in the Shahejie Formation (45.5-28.5 Ma; Guo et al., 2013) of Bohai Bay Basin, which represents a well-preserved middle Eocene unit in China. The Shahejie Formation shales are composed of thick mudstones and shales with interbedded evaporates, containing abundant organic matter (OM) and serving as important source rock for hydrocarbon generation (Allen et al., 1997).

The core samples in this study were collected from a well located in the Gaoliu area of the Nanpu Sag, which is an important hydrocarbon-producing subbasin in the north of the Bohai Bay Basin (Fig. 1). The third member of the middle Eocene Shahejie Formation (Es₃, 45.5–33.7 Ma) is an important suite of source rocks in the Nanpu Sag, and it predominantly consists of dark mudstones and shales interbedded with sandstones and is further divided into five submembers from top to bottom: Es¹₃, Es²₃, Es²₃, Es³₄, and Es⁵₃ (Fig. 2, Dong et al., 2010). Es $_3^4$ (ca. 42.5–42 Ma) contains significant lacustrine shales with high quality OM, hereafter referred to as the MES shales, and contributes large amounts of oil and gas (Zheng et al., 2007; Dong et al., 2010). MES shales were deposited in a semi-deep to deep lacustrine environment (Fig. 2; Zheng et al., 2007; Dong et al., 2010). Under the influence of Pacific plate movement, an obvious unconformity formed at the bottom of Es₃ around 42.5 Ma, with distinguishing features in seismic profiles and well lithology profiles (Xia et al., 2015; Chen et al., 2019). Continuous dense sampling of MES shales provides important material for the investigation of paleoweathering characteristics and paleoclimate evolution in the midlatitudes during the middle Eocene.

3. Methodology

Fifty-three MES shale samples were collected from a 50-m-thick profile (3424.25–3474.08 m) of the continuous drill core of Es_3^4 in well A1 (Fig. 1). This section has not experienced modern weathering. The position of the samples on the stratigraphic column is shown in Fig. 2. All 53 MES shale samples were analyzed by geochemical analysis and were used to evaluate the chemical weathering conditions and climate variation during the middle Eocene in the Bohai Bay Basin. All the tests were performed at State Key Laboratory of Petroleum Resources and Prospecting.

Palynological analysis of *MES shales* was performed using binocular biological microscope. Before observation, the samples were treated with traditional acid and alkali methods (Phipps and Playford, 1984; Xia et al., 2015). The argillaceous and calcareous components in the crushed samples were removed by hydrofluoric acid, and the samples were then neutralized by adding distilled water. After stirring and centrifuging with zinc iodide heavy solution, sporopollen fossils were obtained.

The 53 shale samples were crushed to very fine powder for XRF spectrometry to study the chemical composition. Before each

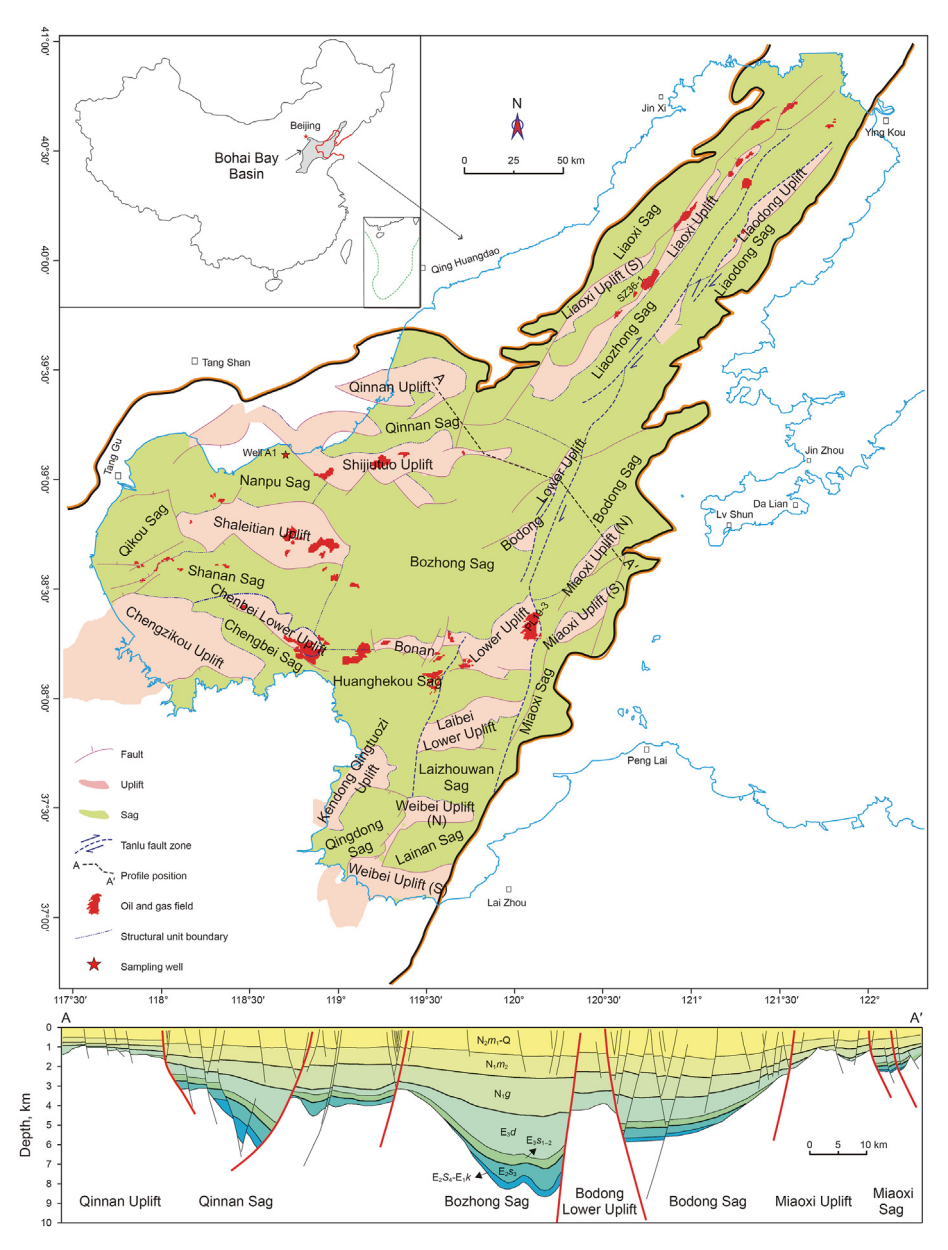


Fig. 1. Geological map and structural profile of the midlatitude Bohai Bay Basin on the eastern side of the Asian continent and the sampling well location (modified from Jiang et al., 2016).

experiment, the shale samples were ground to 200 mesh, oven dried for 2–4 h at 105 °C and cooled. Portions of the samples (0.7 g) were mixed with anhydrous lithium tetraborate, lithium fluoride and ammonium nitrate in a porcelain crucible, stirred well during transfer to a platinum alloy crucible and then dried. Then, the mixture was melted at 1150–1250 °C for 10–15 min and stirred. The resulting melt was cast in a mold to make the sample wafer. Finally, the sample wafer was analyzed with a Shimadzu XRF-1800 X-ray fluorescence spectrometer equipped with a 4.0 kW Rh tube to analyze the spectrum of each major element. Eleven elements were analyzed, and the results are displayed as concentrations in weight percent of the major elements expressed as oxides (SiO₂, Al₂O₃, CaO, Fe₂O₃, K₂O, MgO, MnO, Na₂O, P₂O₅ and TiO₂). The chemical analysis results for the major elements have precisions better than 5% based on replicate and standard analyses.

In addition, spectral analysis technology is used to analyze the periodicity of paleoclimate fluctuation during the middle Eocene based on the no-breaks depositional profile of the MES shales. Spectral analysis is a powerful technique for analyzing the periodicity of various signals, and has been widely used to analyze geological signals. The nonstationary geological signals, such as paleoclimate, river discharge, seismic waves, and sequence stratigraphic divisions, recorded in the sediments are superimposed and feature many different frequencies (Wang et al., 2005). The main frequencies of nonstationary geological signals could be analyzed by wavelet transform, which is an advanced spectral analysis technique based on the Fourier transform and represents an effective method for analyzing the signals in a time series and can provide more frequency information with higher resolutions in terms of frequency and time domains. In this study, discrete wavelet transformation (DWT) is used to process the paleoclimate signal recorded by the chemical composition of the MES shales to identify discrete geological signals. Due to the unequal interval sampling of the MES shales, the signals are resampled, with a

D. Chen, F.-J. Jiang, X.-Q. Pang et al.

Petroleum Science 20 (2023) 1471–1487

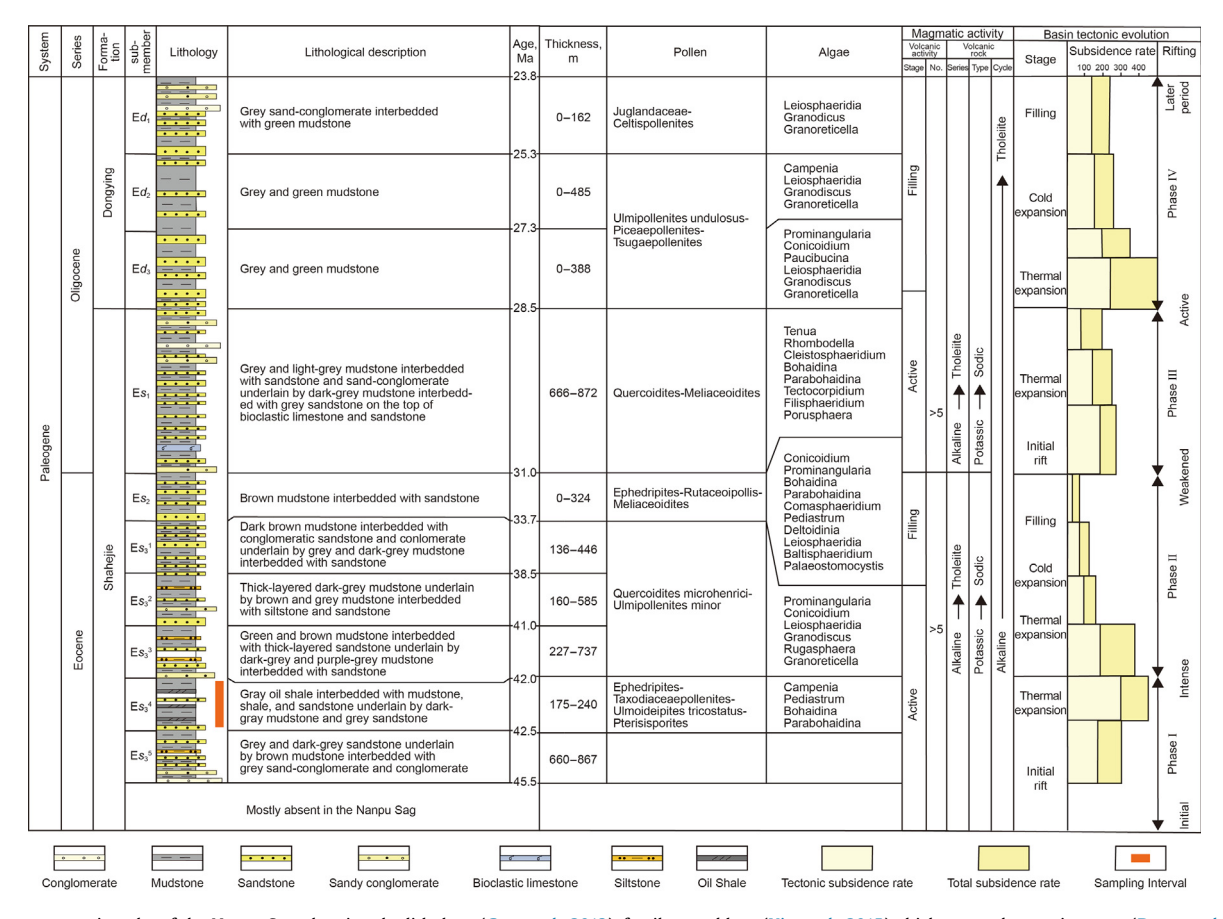


Fig. 2. Paleogene stratigraphy of the Nanpu Sag, showing the lithology (Guo et al., 2013), fossil assemblage (Xia et al., 2015), thickness and tectonic stages (Dong et al., 2010) and sedimentary evolution stages (Jiang et al., 2009).

resampling interval of 0.125 m, to improve the accuracy of this study. Then, the signals are extended to eliminate edge effects, and the extended section is removed after DWT.

4. Results

4.1. Pollen and geologic age

Abundant pollen fossils were identified in MES shales, and the details are shown in Fig. 3. Angiospermae pollen dominates at 57.8 to 93.6%, followed by Gymnospermae (6.4%–42.2%). Pteridophyta are rare. Amongst Angiospermae pollen, Quercoidites dominates at 13.9–42.4%, followed by Ouercoidites microhenrici (4.1%–28%). Ulmipollenites and Ulmoideipites (8.3%–26%), Juglandaceae (2%– 20.2%) and Betulaceae (4.4%–19.7%). Quercoidites prefer subtropical climate, and Ulmipollenites are mostly developed in temperate climate regions. Preponderant Quercoidites and Ulmipollenites in MES shales reflect the subtropical to temperate climate during depositing phase, which also occur in Es4 sediments of Liaohe, Jiyang and Dongpu Depressions in the Bohai Bay Basin (Zhang et al., 2016). Furthermore, *Ulmipollenites undulosus* varies between 2.7% and 8.5%, Juglanspollenites varies between 2% and 12.8%, Betulaceoipollenites between 2.2% and 11.5%, and Momipites between 2.2% and 11.8%. Liquidambarpollenites (1.5%-11.5%) and Tricolporopollenites (1.6%–5.9%) are also common in MES shales. In addition, few Alnipollenites, Faguspollenites, Caryapollenites, Ulmipollenites minor, Ulmoideipites tricostatus, Quercoidites minutus, Chenopodipollis, Rutaceoipollenites, Labitricolpites, Magnolipollis, Meliaceaeoidites have been distinguished in MES shales. Gymnospermae pollen

is predominated by *Pinaceae* (1.1%–25.8%) and *Taxodiaceae* (1.6%–11.7%), followed by *Pinaceae* (1.1%–17.2%), *Abietineaepollenites* (0–6.9%), *Taxodiaceo pollanites* (0–6.8%) and *Ephedripites* (0–11.7%). The appearance of *Ephedropites* indicates that there was a dry and hot climate at that time, which is similar to the climate and *Ephedropites* records of Es₃ sediments in Dongpu Depression (Zhang et al., 2016). Few *Cedripites* and *piceaepollenites* were found in this study. The content of *Pteridophyta* pollen is very low (0–3.1%), and several *Alsophilidites*, *Deltoidospora* and *Polypodiaceaesporites* have been identified. Furthermore, relatively abundant algae fossils have also been discovered in *MES shales*. *Leiosphaeridia* and *Pediastrum* are the most common in *MES shales*, and *Parabohaidina*, *Conicoidium*, *Cleistosphaeridium*, *Membranilarnacia*, *Comasphaeridium*, *Granodiscus*, *Campenia* and *Filisphaeridium* were also found in this study.

Quercoidites, Quercoidites microhenrici and Quercoidites minutus usually occurred in the Eocene and later sediments, and they are widespread in China, Europe and North America (Wang et al., 2003). Decline of apertured pollen, absence of archaic Normapolles and Aquilapolles, as well as increase in Tricolporopollenites assembly are features of middle Eocene (Song and Liu, 1983). Higher amounts of Quercoidites are a representative feature for the Eocene Shahejie Formation in the Bohai Bay Basin (Zhang and Yin, 2005; Xia et al., 2015). The occurrence of Tricolporopollenites (2–5.9%) suggests that the shales in this study belongs to the middle Eocene. These assemblages of pollen and algae and their variations in this study are consistent with the combination of Ephedripites- Taxodiaceaepollenites- Ulmoideipites tricostatus- Pterisisporite in the previous study by Xia et al. (2015), which belong to

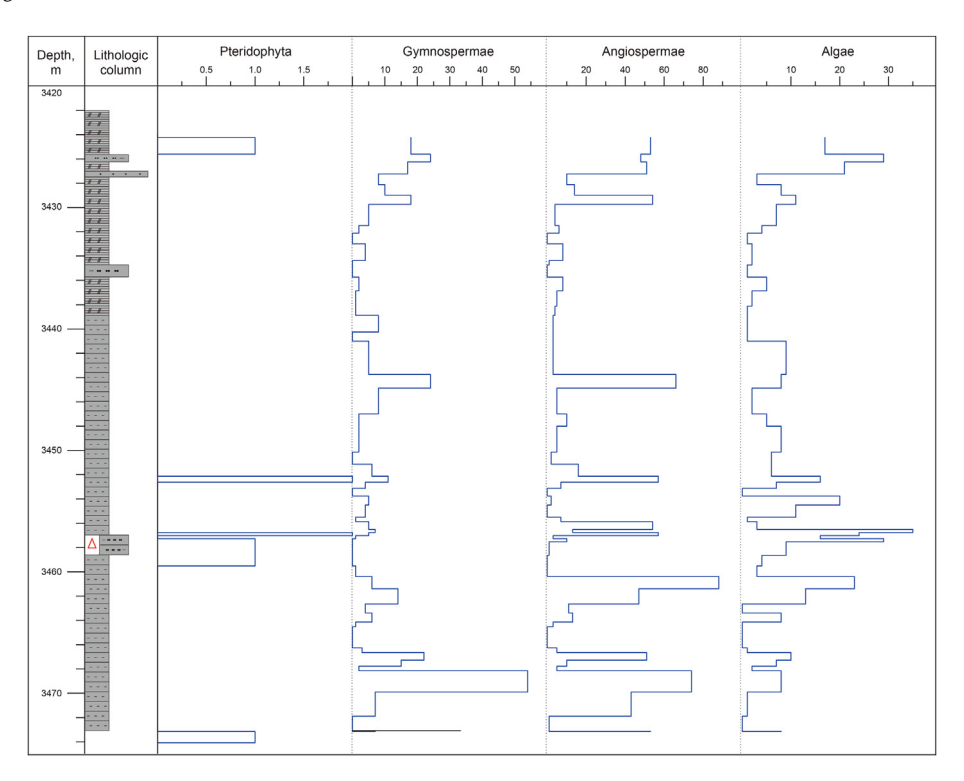


Fig. 3. Palynological diagram and assemblage in the MES shales.

the Es⁴₃ stratum. In addition, the assemblages of pollen in *MES shales* are similar to those in the Es³ sediments in Dongying sag, suggesting the warm and humid climate (Lei et al., 2018).

4.2. Major elements and mineral composition

The elemental concentrations of the *MES shales* are shown in Fig. 4a. Overall, the predominant major element is SiO₂ (ranging from 28.51 to 64.19 w.t.%, average: 49.60 w.t.%), followed by CaO

 $(1.12-35.24 \text{ w.t.\%}, \text{ average: } 13.62 \text{ w.t.\%}), \text{ Al}_2\text{O}_3 (5.56-17.85 \text{ w.t.\%}, \text{ average: } 12.67 \text{ w.t.\%}), \text{ and } \text{Fe}_2\text{O}_3 (3.12-15.43 \text{ w.t.\%}, \text{ average: } 6.97 \text{ w.t.\%}), \text{ with lesser amounts of MgO } (1.53-5.61 \text{ w.t.\%}, \text{ average: } 2.58 \text{ w.t.\%}), \text{ K}_2\text{O } (0.88-3.50 \text{ w.t.\%}, \text{ average: } 2.28 \text{ w.t.\%}), \text{ Na}_2\text{O } (0.43-1.87 \text{ w.t.\%}, \text{ average: } 1.01 \text{ w.t.\%}), \text{ TiO}_2 (0.28-0.88 \text{ w.t. \%}, \text{ average: } 0.63 \text{ w.t.\%}), \text{ P}_2\text{O}_5 (0.17-1.98 \text{ w.t.\%}, \text{ average: } 0.77 \text{ w.t.\%}), \text{ MnO } (0.02-0.47 \text{ w.t.\%}, \text{ average: } 0.16 \text{ w.t.\%}), \text{ and } \text{SrO } (0.05-0.24 \text{ w.t.\%}, \text{ average: } 0.12 \text{ w.t.\%}).$

To compare these results with the average values of the upper

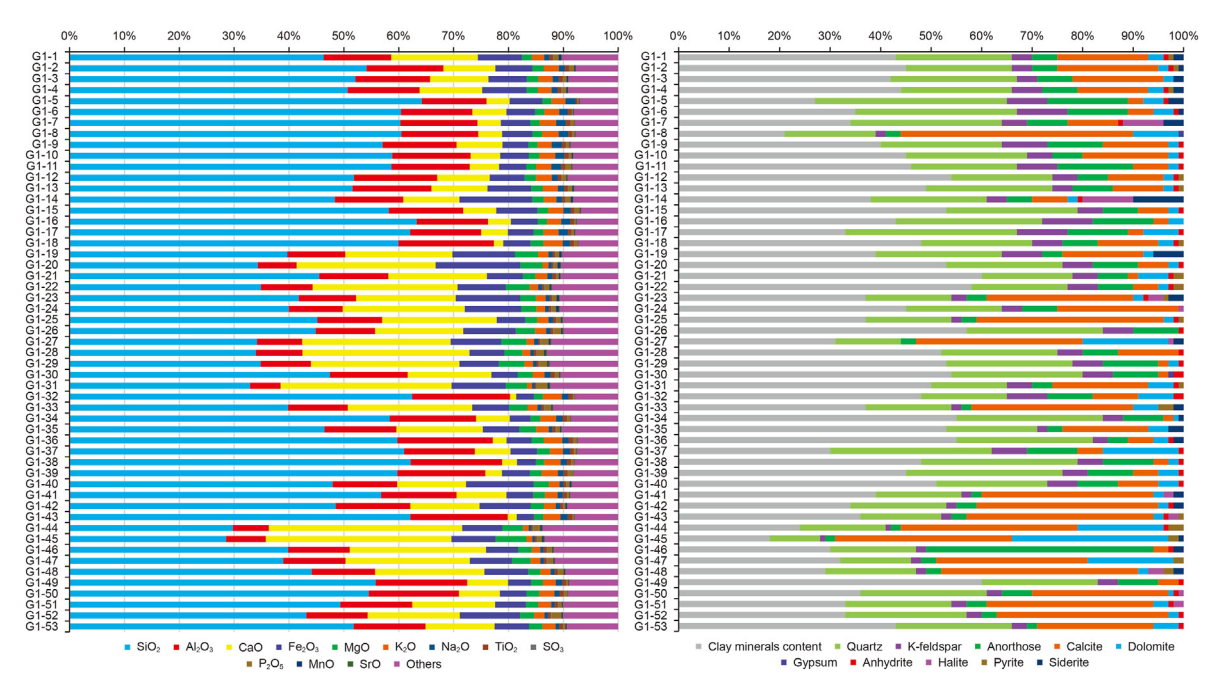


Fig. 4. wt percentages of major elements (a) and mineral composition (b) of the MES shales. The mineral composition data are derived from Chen et al. (2019).

D. Chen, F.-J. Jiang, X.-Q. Pang et al.

Petroleum Science 20 (2023) 1471–1487

continental crust (UCC), the major element compositions of the MES shale samples were normalized to the UCC composition (Taylor and McLennan, 1985), and the diagrams are shown in Fig. 5, which shows the gain or loss of elemental mass relative to the UCC. Values > 1 indicate an increase in the relative abundance of the element in the sample compared to the UCC, whereas values < 1 indicate a decrease in the relative abundance of the element. mainly due to the paleoweathering processes (Perri and Ohta, 2014). In this study, the values of SiO₂, Al₂O₃, K₂O and Na₂O are less than 1, implying that the formation of the MES shales involved moderate weathering of continental crustal material. Si, Al and K are typical incompatible elements and important components of chemically stable minerals, such as quartz and feldspar, which are commonly concentrated in geochemically mature sediments (Khudoley et al., 2001; Ohta, 2004; Perri and Ohta, 2014). This result suggests that the Bohai Bay Basin most likely experienced active tectonic conditions during the middle Eocene. The strong depletion in Na and positive correlation between Na₂O and SiO₂ (Fig. 6a) implies intense dissolution of albite, which is the main host mineral of the Na⁺ mobile cation (Fig. 6a–b).

Calcium is highly enriched in the MES shales compared to the UCC, as shown in Fig. 5. The positive correlations between P₂O₅ and CaO and between SO₃ and CaO (Fig. 6d-e) indicates that these elements may be present as apatite and anhydrite/gypsum. This result is confirmed by the mineral components (Fig. 6b) and XRD result (Fig. 4). The presence of anhydrite indicates that it was in a torrid evaporation environment. However, the correlations between P₂O₅ and SO₃ and CaO are only weakly positive with relatively high scatter, hinting that additional CaO may reside in carbonates (Fig. 6e-f). In addition, CaO is negatively correlated to both Al₂O₃ and SiO₂ (Fig. 6b-c), suggesting a possible source of CaO from silicate and carbonate minerals. The CaO content is several times higher than the MgO content with a positive relationship (Fig. 6f), suggesting that calcite is dominant over dolomite among carbonates, which is also supported by mineralogical composition (Figs. 6 and 4b).

 Al_2O_3 has a positive relationship with K_2O (Fig. 6g), indicating that both K and Al are most likely incorporated into the mineral illite (Gabbott, 1998). The positive correlation between SiO_2 and Al_2O_3 suggests that the primary host of Si may be clay minerals (Fig. 6h—g). In this study, a good positive correlation exists between TiO_2 and Al_2O_3 (Fig. 6i). The fairly constant Al/Ti ratio indicates that

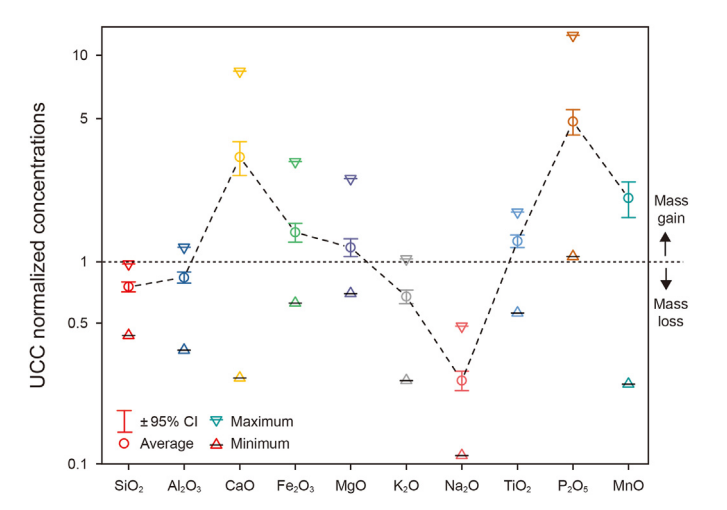


Fig. 5. Mass-balance calculation for major elements in the *MES shales* compared to the UCC. The UCC normalized concentrations refers to the ratio of measured oxide content to that in UCC which is derived from Taylor and McLennan (1985).

Ti is mainly incorporated into the structure of clay minerals or occurs as hydroxides or oxides (Young and Nesbitt, 1998; Panahi et al., 2000).

These results are consistent with the mineralogical composition reported in previous study about *MES shales* (Fig. 4b; Chen et al., 2019). The minerals in *MES shales* are dominated by clay minerals, and followed by quartz, feldspar and carbonates. Furthermore, orthoclase and albite could be observed in *MES shales*. Calcite is dominant amongst carbonates, followed by dolomite. The main clay minerals include illite and smectite. Moreover, minor gypsum, pyrite, siderite, apatite and so on could also been observed in *MES shales*. The morphology of these minerals could be observed as in Fig. 7, and some dissolutions were also presented in *MES shales*.

4.3. Weathering characteristics and paleoclimate conditions

Chemical weathering strongly affects the geochemical and mineralogical variability of sedimentary rocks (Nesbitt et al., 1996). Chemical weathering, which is mainly mediated by the climate conditions, converts primary labile silicate minerals to secondary clay and oxide-hydroxide minerals by releasing mobile elements, such as sodium, calcium and potassium, from silicate minerals. Paleoweathering processes can be quantified by the chemical index of alteration (CIA), which was proposed by Nesbitt and Young (1982) as follows:

$$CIA = [Al_2O_3 / (Al_2O_3 + CaO^* + Na_2O + K_2O)] \times 100$$
 (1)

CaO* is the amount of CaO present in the silicate fraction of the rock. In this study, CaO in phosphate was corrected (McLennan, 1993). In addition, a reasonable CaO/Na2O ratio was proposed to indirectly estimate the CaO in the silicate fraction by distinguishing it from carbonate CaO directly (McLennan, 1993; Bock et al., 1998). When $CaO > Na_2O$, $CaO^* = Na_2O$; and when $CaO \le Na_2O$, CaO* = CaO. The CIA is a dimensionless parameter ranging from 0 to 100. Generally, high CIA values indicate the removal of mobile elements (e.g., Ca²⁺, Na⁺, and K⁺) relative to stable conservative elements (Al³⁺ and Ti⁴⁺) due to chemical weathering under humid and warm climate conditions, in which secondary minerals, such as kaolinite, are produced. Therefore, higher CIA values correspond to increasing chemical weathering and sediment maturity. In contrast, very low CIA values reflect the absence of source-area weathering and low sediment maturity and deposition under cool and/or arid conditions (e.g., Rieu et al., 2007; Perri, 2018). CIA values of 45-55 indicate no weathering, while a CIA value of 100 indicates intense weathering. CIA values between 50.0 and 60.0 indicate a low degree of chemical weathering, values ranging from 60.0 to 80.0 indicate moderate weathering, and values > 80.0 indicate extreme chemical weathering (Nesbitt and Young, 1982; Fedo et al., 1995, 1996). In this study, the CIA values of the MES shales range from 57.3 to 75.5, with an average of 69.2. The CIA values of MES shales are significantly higher than that of the UCC (47.7), but similar to that of post-Archean Australian shales (PAAS) (70.3; Taylor and McLennan, 1985, Fig. 8a). The results are also supported by the relative high content of Ulmipollenites Betulaceoipollenites and Juglanspollenites in the Angiospermae pollen of the MES shales. The CIA values of EMS shales are lower than those of the Es₃ sediments in Dongying sag (avg. 81.6), while are similar to the CIA values of the evaporite interlayer in the Es^U₄ sediments of Dongying sag (63.1–84.0, avg. 69.4). This feature reflects the relative dry climate and weakmoderate weathering during the MES shales depositing (Ma, 2017).

In addition, based on the proportion of secondary aluminous minerals relative to primary mineral phases, the Al₂O₃-(CaO*+Na₂O)-K₂O (A-CN-K, Fig. 8a) ternary plot has been widely used to analyze the weathering rates of primary minerals and

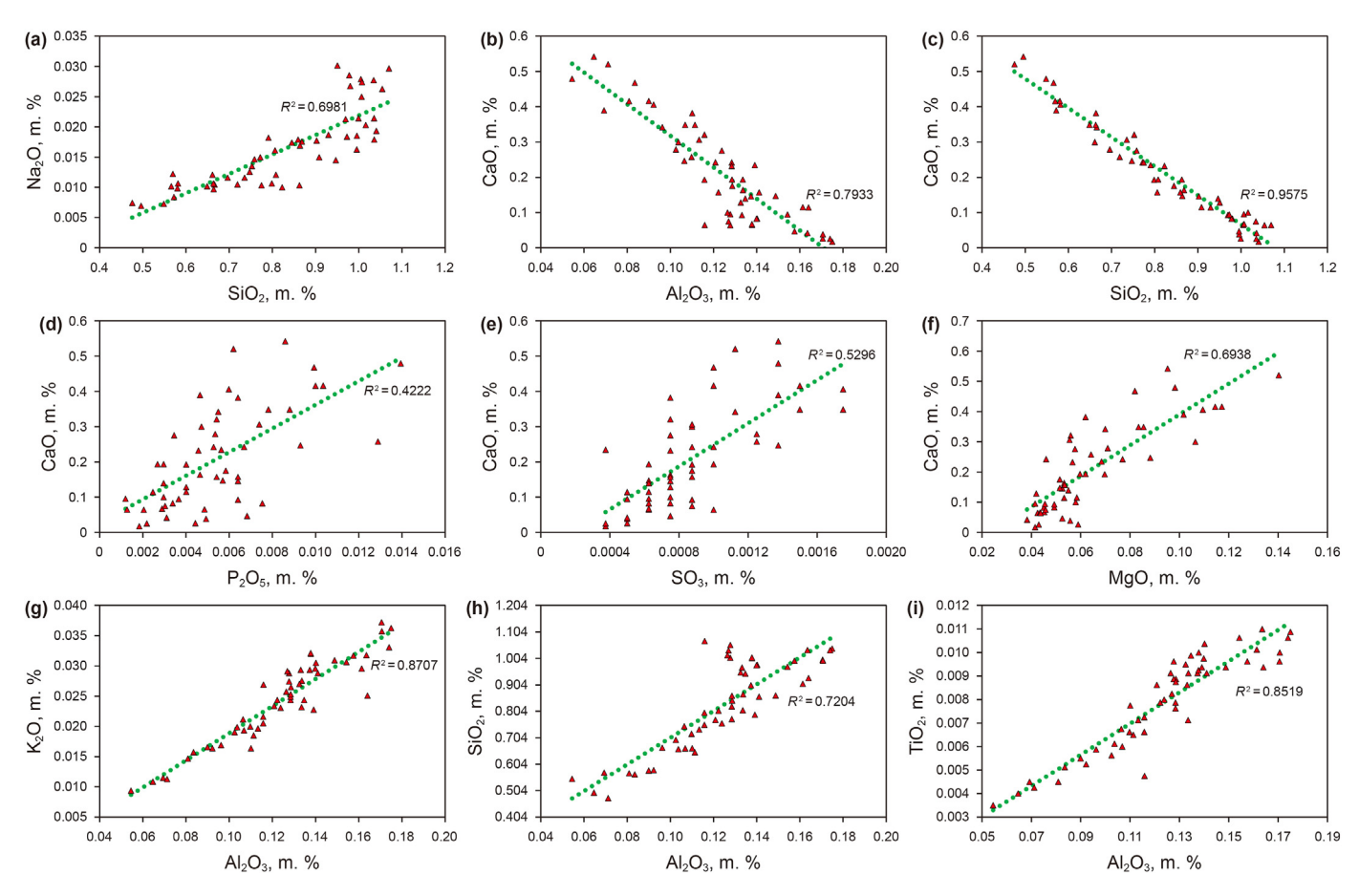


Fig. 6. Correlations among the major element oxides (in molar proportions) in the *MES shales*. (a) shows a positive correlation between Na₂O and SiO₂. CaO show negative correlations with Al₂O₃ (b) and SiO₂ (c), but positive correlations with P₂O₅ (d), SO₃ (e), and MgO (f). Analogously, good positive correlations were presented in K₂O vs. Al₂O₃ (g), SiO₂ vs. Al₂O₃ (h) TiO₂ vs. Al₂O₃ (i).

weathering-induced diagenetic alteration (Nesbitt and Young, 1984, 1989; Panahi et al., 2000). In this diagram, A, (C + N) and K are in molar values. The progress of weathering on such diagrams is generally shown along straight lines subparallel to the A-CN line. Almost all of MES shale samples were plotted on the straight line subparallel to A-CN (Fig. 8a). This reflects that sediments have been subjected to different degrees of chemical weathering, leading to the predominant removal of silicate Ca and Na due to the destruction of plagioclase feldspars (Nesbitt and Young, 1982, 1984; Újvári et al., 2014). This plots along the predicted weathering trend, indicates Ca²⁺ and Na⁺ leaching via moderate weathering processes. Furthermore, the weathering trend resulted in the formation of some minerals that are compositionally between illite and kaolinite (Fig. 8a). No obvious tendency towards the K₂O vertex is observed for MES shales, suggesting little K-metasomatism participated in the chemical weathering process (Fedo et al., 1995). Furthermore, a quantitative method has been proposed to calculate K₂O addition by Panahi et al. (2000):

$$K_2 Ocorr = \left[m \times A + m \times (C^* + N) \right] / (1 - m) \tag{2}$$

$$M = K / (A + C^* + N + K)$$
 (3)

where m could be obtained from a line emanating from the plotted points and parallel to the A-CN line (Fig. 8a), and m=0.14 in this study. The K₂Ocorr values of the MES shales are low (0.01–0.03; avg. 0.02), indicating weak and negligible K-metasomatism in the weathering process.

The geochemical weathering conditions can also be predicted by the M-F-W ternary diagram, which was developed from a statistical analysis of element behavior during the course of igneous rock weathering (Ohta and Arai, 2007). M and F represent mafic and felsic igneous source rocks respectively, and W represents the degree of weathering (Ohta et al., 2011). This method takes into account eight major elements, and it is more reliable and sensitive to weathering trends than conventional indices based on two to four element oxides. In this study, the W values of the MES shales range from 31.02 to 69.02 with an average of 54.64, and it has a strong positive correlation with the CIA (Fig. 10a), suggesting its good reliability for identifying weathering conditions. The MES shales plots show a trend toward the W vertex (Fig. 8b), indicating moderate weathering condition. The W values of the MES shales are equivalent to those of recent soils that developed in midlatitude regions with a temperate climate (Ohta et al., 2011; Perri and Ohta, 2014, Fig. 9). Although the MES shales in this study are not consistent with paleosol, its W values are distinctly different from those of soils that developed in arctic, boreal temperate and tropical rainforest climates, implying that the MES shales sediments experienced a temperate climate during the middle Eocene. This result is also supported by the relatively high content of Ulmipollenites, Betulaceoipollenites and Juglanspollenites in the Angiospermae pollen. In addition, Quercoidites dominate in the MES shales, and this genus is regarded as a representative subtropical pollen that show a preference for subtropical climates.

D. Chen, F.-J. Jiang, X.-Q. Pang et al. Petroleum Science 20 (2023) 1471–1487

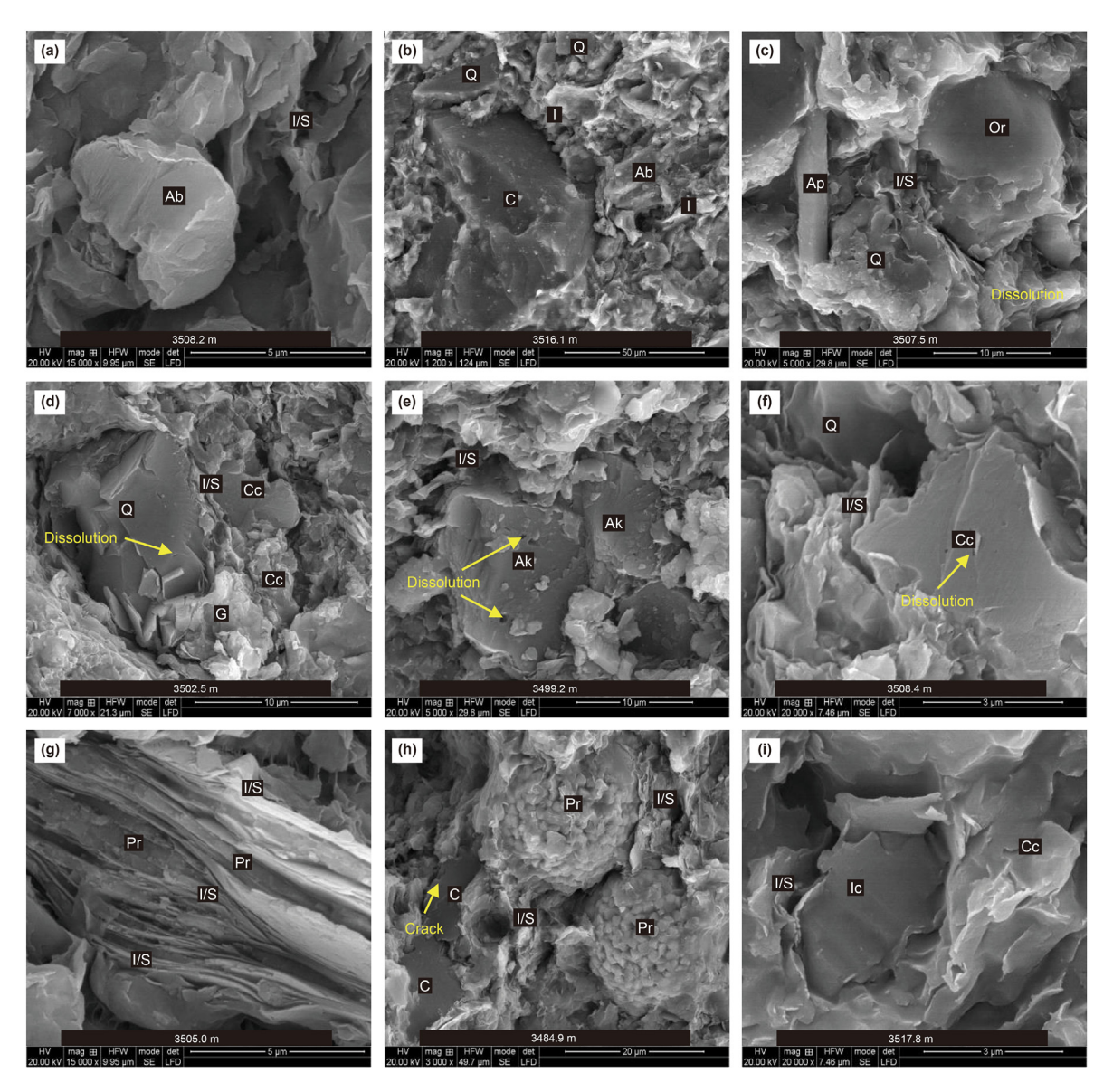


Fig. 7. The mineral morphology of MES shales from scanning electron microscopy observation. The minerals include quartz (Q), pyrite (Pr), illite (I), illite/smectite mixture (I/S), orthoclase (Or), calcite (Cc), feldspar (Fs), albite (Ab), ankerite (Ak) and OM (C). Some cracks and dissolution could also been observed.

4.4. Paleotemperature and paleoprecipitation

In the chemical weathering process, the mobile alkaline cations of alkaline aluminosilicates, i.e., Na⁺, K⁺, and Ca²⁺, are depleted because the dissolved carbonic and organic acids present in meteoric water and surface water transform these aluminosilicates into clay minerals. This process is primarily controlled by the prevailing climate, including the surface temperature and precipitation regime (Muhs et al., 2001; Sheldon et al., 2002; Passchier et al., 2013, 2017), and leads to geochemical and mineralogical variability in sedimentary rocks.

By analyzing the different molar oxide ratios of K, Na, and Ca versus Al in the soil weathering horizons in North America, Sheldon et al. (2002) proposed the mean annual temperature (MAT) and mean annual precipitation (MAP) as two climofuctions to reconstruct the paleoclimate under which paleosols formed, and the results are comparable to other independent proxies. This method has been used by Passchier et al. (2013, 2017) to reconstruct Antarctic continental paleotemperature and precipitation during the

Eocene and Miocene. The mean annual temperature is calculated as MAT = -18.516(S) + 17.298, where S is defined as the molar ratio of Na_2O and K_2O to Al_2O_3 . For MAP (mm/yr), Passchier et al. (2013) modified the climofunction based on Sheldon et al. (2002) to emphasize the silicate mineral-bound components: $MAP = 147.75 \times exp(0.0232 \times CIA-K)$, where CIA-K is the CIA without potassium (potassium is excluded to remove the effects of potassium metasomatism on paleosols; Maynard, 1992).

For the MES shales (Fig. 10), the MAT values range from 8.3 °C to 12.9 °C with an average of 11.3 °C. The MAP values are in the range of 685.2–1099.8 mm/yr (avg. 946.5 mm/yr), suggesting that the Bohai Bay Basin suffered seasonally dry and humid conditions (600–1200 mm/yr; Sheldon et al., 2009) during the middle Eocene. Furthermore, these values are obviously lower than those associated with tropical conditions, which have annual rainfall totals of 2500–3750 mm (Nesbitt and Young, 1989). This result is also supported by pollen. The content of helophytes, such as *Polypodiaceaesporites*, *Taxodiaceaepollenites*, and *Alnipollenites*, are lower than that of *Ephedripites* in *MES shales* indicating that a

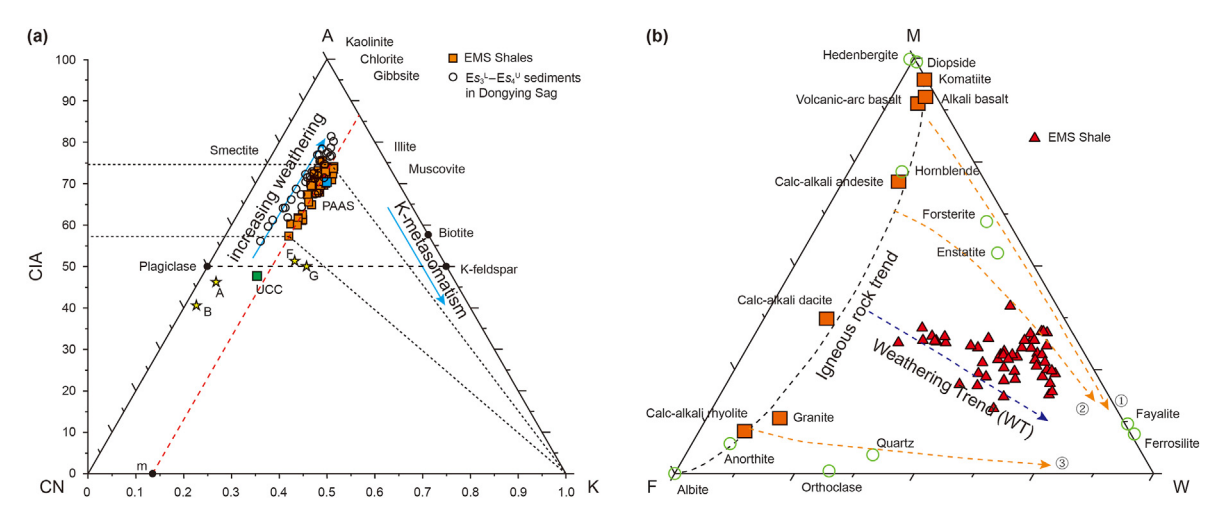


Fig. 8. Geochemical weathering trends of the MES shales. (a) A-CN-K (Al_2O_3 – $CaO^* + Na_2O$ – K_2O , all in molar proportions) ternary diagram showing the weathering trend of the MES shales, with the chemical index of alteration (CIA) scale on the left. Yellow stars: A, andesite; B, basalt; F, felsic igneous rock; and G, granite (Condie, 1993). UCC, upper continental crust; PAAS, post-Archean Australian shales (Taylor and McLennan, 1985). (b) Weathering trends of the MES shales depicted on the M-F-W diagram (Ohta and Arai, 2007). The M, F and W vertices represent unweathered mafic igneous rocks, felsic igneous rocks and weathering degree of these parent igneous rocks, respectively. The black dashed line represents a compositional linear trends for the weathering of basalt, diorite and granite.

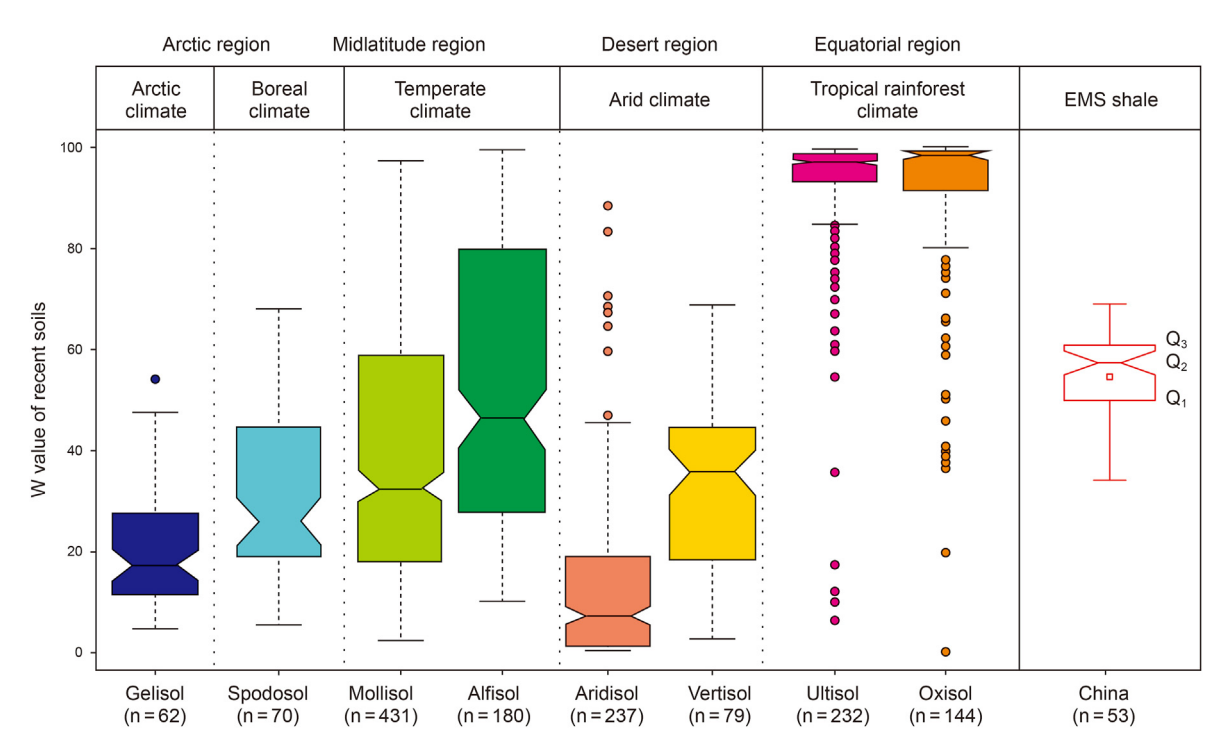


Fig. 9. Comparison of the W values of recent soils developed under various climate regimes (Ohta et al., 2011) and those of the MES shales. The W values of the MES shales in the Bohai Bay Basin are comparable to the soils developed in temperate climates in the midlatitude region. For each box plot, the lower and upper limits represent the first (Q_1) and third (Q_3) quartiles and the line within the box represents the second (Q_2) quartile. The small block within the box represents the mean value. The widths of notches on the side of each box indicate the 95% confidence intervals of the median (Ohta et al., 2011). Whiskers represent the allowable range of the data (1.5 times the interquartile range). Solid circles represent outliers.

transitory moist climate occurred along with the persistent seasonal climate.

The maximum value is below the upper limits of MAT > 18 °C or MAP > 1600 mm/yr, which correspond to the complete leaching of labile minerals (Sheldon et al., 2002; Passchier et al., 2013). The MAP and MAT trends of the midlatitude Bohai Bay Basin during the middle Eocene calculated in this study are similar to those of the high-latitude Antarctic continental margin calculated by Passchier et al. (2013; Fig. 11) and show the same magnitude, despite the considerable geographic differences. In addition, the MAP and MAT

trends both decrease (Fig. 11) during the middle Eocene over a short time scale of 42.5-42 Ma. In addition, the MAT and MAP are positive correlated with the CIA (Fig. 10b—c), which supports the above explanation of the CIA.

5. Discussion

5.1. Provenance, tectonics and sediment maturity

Provenance and tectonics are important factors that affect

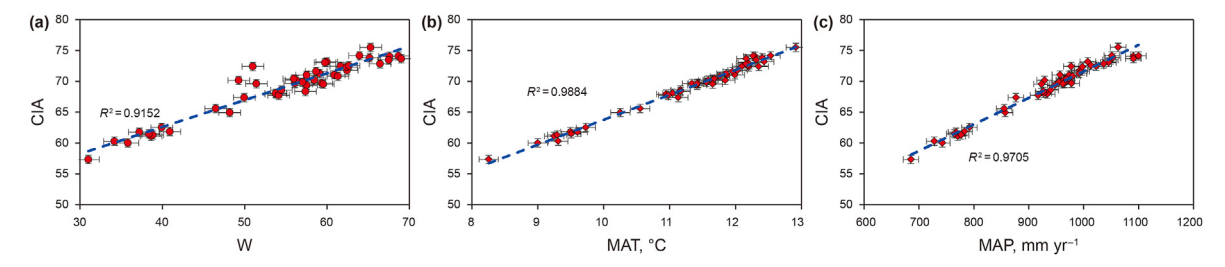


Fig. 10. (a) Shows a positive relationship between the CIA and the W index. Positive relations of CIA with MAT (b) and MAP (c).

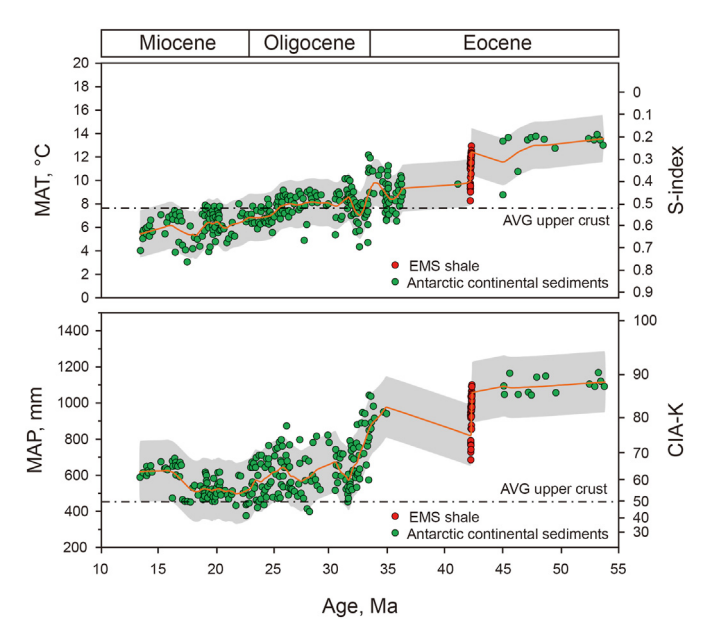


Fig. 11. Comparison of MAT and MAP under the high latitude regime (Passchier et al., 2013) and for the *MES shales* in the midlatitude Bohai Bay Basin. The MAT and MAP of the *MES shales* are consistent with their variation trend during the Eocene calculated from the detrital geochemistry of the Antarctic continental margin. Gray shadings present prediction intervals at $\alpha=0.05$ level. The orange smoothing trendline is derived by using the Locally Weighted Scatterplot Smoothing algorithm.

weathering products (Armstrong-Altrin and Verma, 2005; 2013; Awasthi, 2017). The A-CN-K plots show moderate paleoweathering for the MES shales relative to the UCC and PAAS, and the provenances are close to mafic and felsic igneous rocks (Fig. 8a). Furthermore, the M-F-W diagram suggests that the provenance of the MES shales was intermediate in composition (Fig. 8b). To identify the provenance of the MES shales more exactly, a discrimination diagram based on seven major element compositions proposed by Roser and Korsch (1988) is further used in this study. As shown in Fig. 12a, the MES shales are mainly located in the P2 field, followed by the P1 and P3 fields. This pattern implies a mainly intermediate provenance and less mafic and felsic sources. This result also is supported by the Al₂O₃/TiO₂ ratio of 16.92–31.11 (avg. 20.30), which indicate a provenance from intermediate igneous rocks (Hayashi et al., 1997).

Furthermore, the *MES shales* are mainly immature and formed in an active continental margin and island arc tectonic setting (Fig. 12a; Roser and Korsch, 1988; Roser et al., 1996). This tectonic background is further supported by the K₂O/Na₂O vs. SiO₂ diagram (Fig. 12b; Roser and Korsch, 1986) and Al₂O₃/SiO₂ vs. Fe₂O₃ and MgO diagram (Fig. 12c). Due to the subduction roll-back of the Pacific Plate relative to the eastern margin of Asia, many extensional basins with similar ages and structural styles formed on the

eastern side of the Asian continent from Russia to Vietnam (Allen et al., 1997). These active continental margin basins and associated island arcs are typical of the western Pacific Plate (Allen et al., 1997). The Bohai Bay Basin is one of these active continental margin basins associated with extensive regional normal-slip and strikeslip faulting. To some extent, active tectonics can produce sedimentary recycling (Armstrong-Altrin and Verma, 2005; Hao et al., 2010; Awasthi, 2017), which is an important factor that can change the bulk chemical and mineralogical composition of sedimentary rocks. To ensure the accuracy of the weathering reconstruction, first-cycle deposits are preferred. Sedimentary recycling can be distinguished by the index of compositional variability (ICV) proposed by Cox et al. (1995):

$$ICV = (Fe_2O_3 + K_2O + Na_2O + CaO + MgO + MnO + TiO_2) / Al_2O_3$$
(4)

where the weight percentages of the oxides are used. The ICV was applied to estimate compositional maturity and has been used to track sediment recycling. When ICV > 1, the sediments are compositionally immature first-cycle deposits, which tend to be found in tectonically active settings. In contrast, compositionally mature sediments have low ICV values (ICV < 1). These sediments are associated with active sediment recycling under quiescent or cratonic environments. They may also be produced by chemical weathering of first-cycle sediments (Cox et al., 1995; Perri and Ohta, 2014). The MES shale samples generally have ICV values of > 1, suggesting that the MES shales were compositionally immature or low-mature first-cycle deposits. Therefore, the chemical and mineralogical composition of the MES shales could effectively reflect the chemical weathering condition of its source area during the middle Eocene.

The low compositional maturity of *MES shales* could be further verified by the SiO₂/Al₂O₃ ratio. The SiO₂/Al₂O₃ ratio reflects the abundances of quartz and clay/feldspar, and is sensitive to weathering and sediment recycling. Thus, this ratio can also be used to estimate the degree of sediment maturity. Higher SiO₂/Al₂O₃ ratios indicate the higher maturity due to increase in modal framework quartz at the expense of less resistant components of feldspar (Potter, 1978; Roser et al., 1996; Hao et al., 2010; Fadipe et al., 2011; Fatima and Khan, 2012; Babeesh et al., 2017). The SiO₂/Al₂O₃ ratios of the *MES shales* are typically low (Roser et al., 1996), ranging from 3.31 to 5.92 (avg. 3.97). These values are close to that of PAAS (3.32), suggesting that the *MES shales* are immature sediments derived from a mixed provenance.

Overall, the *MES shales* feature a mixed provenance that consists of intermediate igneous rocks. Due to the active tectonics during the middle Eocene, the *MES shales* represent an immature first-cycle deposits. Under a subtropical and seasonal climate, the *MES shales* experienced moderate chemical weathering during the middle Eocene.

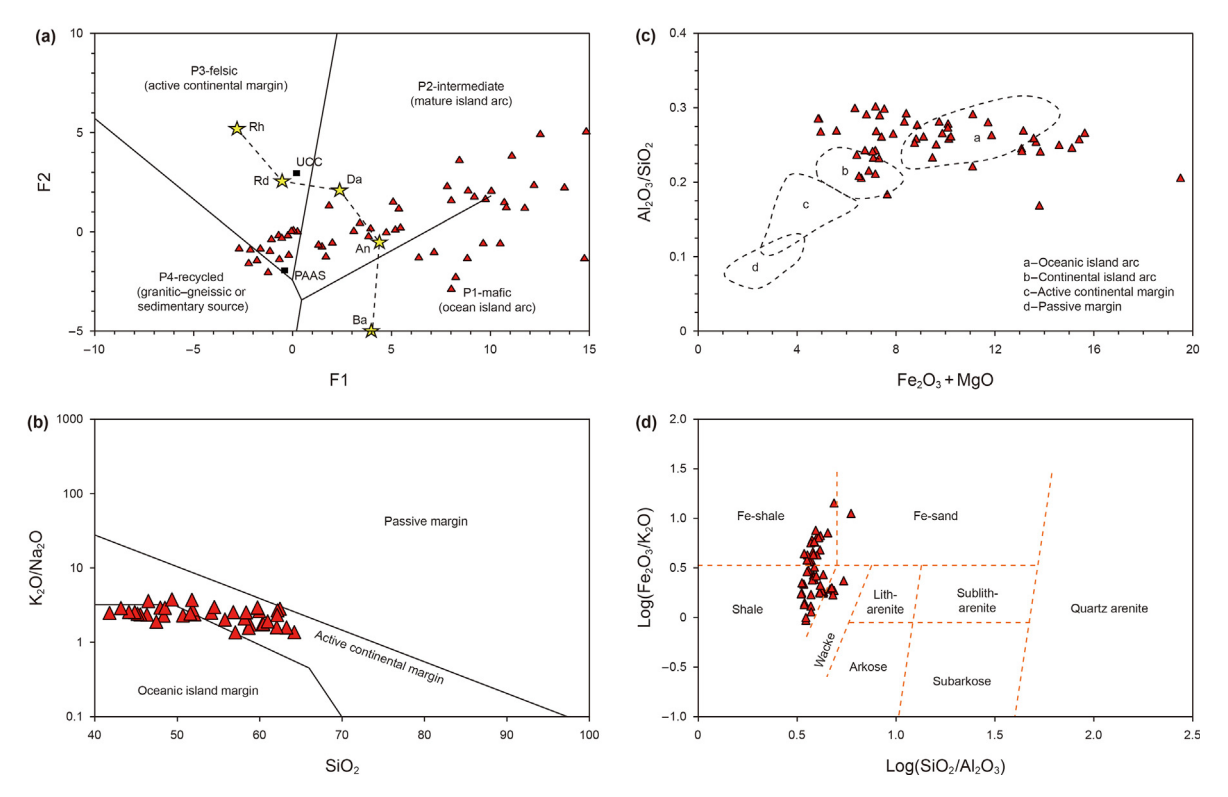


Fig. 12. Provenance and tectonic discrimination plots for the MES shales (red solid triangle in subfigure). (a) Provenance discrimination diagram for the MES shales using the discrimination diagram proposed by Roser and Korsch (1988); stars Rh, Rd, Da, An, and Ba represent the average rhyolite, rhyodacite, dacite, andesite and basalt, respectively. (b) and (c) show the evaluation of tectonic settings of the Bohai Bay Basin by the SiO₂–K₂O/Na₂O (Roser and Korsch, 1986) and Fe₂O₃+MgO–Al₂O₃/SiO₂ diagrams (Bhatia, 1983). (d) shows the geochemical classification of the MES shales using the log(SiO₂/Al₂O₃) - log(Fe₂O₃/K₂O) diagram (Herron, 1988).

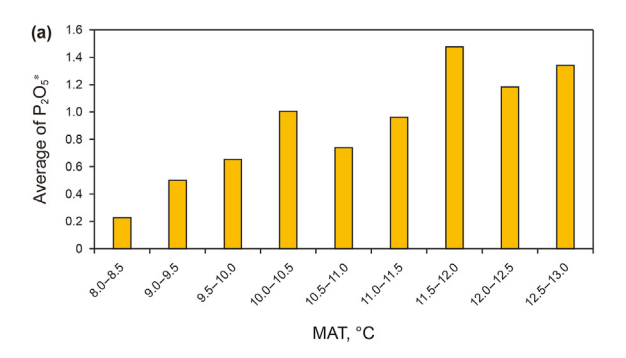
5.2. Organic matter implications

In addition to influencing chemical weathering, the climate also influences the status of lakes. The primary productivity and fertility of lakes are tightly associated with phosphate (Schindler, 1975; Smith, 1983; Hecky and Kilham, 1988; Howarth et al., 1988). The availability of phosphorus is critical to the OM production (Spears et al., 1988; Ward et al., 1996). The presence of phosphorous enhances the growth of algae/vegetation, and the resulting OM can then be preserved in reducing depositional environments (Ward et al., 1996; Tao et al., 2012).

High-vitrinite sediments always have high phosphorus levels (Ward et al., 1996), and phosphorus precipitation has a good positive correlation with the total organic carbon (TOC) content (Chen et al., 2006). The phosphorus contents of the MES shales are 0.07-0.86 w.t.% (avg. 0.34 w.t.%; Fig. 4a), which is higher than that in the UCC and PAAS (both 0.17 w.t.%; Taylor and McLennan, 1985). The phosphorus content of dried modern plants is typically approximately ten times that of sediments (Ward et al., 1996). Hence, the phosphorus content found in coal seams is probably less than that in the original vegetation that formed the peat accumulations (Ward et al., 1996). The phosphorus contents in the MES shales are higher than those in coals (Ward et al., 1996), indicating a high degree of nutrient availability and productivity in the Bohai Bay Basin during the middle Eocene. Furthermore, the P₂O₅* index was used by Schmitz et al. (1997) to monitor the biological productivity during the latest Paleocene benthic extinction event. P₂O₅* is the concentration of phosphate in a sample normalized to the UCC values. It is calculated as $P_2O_5^* = (P_2O_5/Al_2O_{3wr}) \times$ Al₂O_{3UCC}, where Al₂O_{3wr} is the measured Al₂O₃ and Al₂O_{3UCC} is the average Al₂O₃ content of the UCC with a value of 15% (Schmitz et al., 1997). The P₂O₅* values of MES shales range from 0.20 to 5.34, with

a mean of 1.07, indicating that the *MES shales* were deposited in a nutrient-rich environment along with abundant OM. The relationships of P_2O_5* with MAP and MAT (Fig. 13a–b) shows that values of 11.5–12 °C and 1000–1050 mm/yr prefer to phosphate enrichment.

P₂O₅* is positive related with ICV (Fig. 14a), which suggests that the OM accumulation and primary production in paleolakes were associated with tectonic activity companying with higher terrestrial inputs. A weak positive correlation was presented between P₂O₅* and TOC (Fig. 14b), which may be affected by redox condition of sedimentary water and sediment bulk accumulation rates (Schoepfer et al., 2015). The relatively oxidized underwater environment has found low ratio of organic carbon and organic phosphorus mass fraction with high productivity, (Canfield, 1994). Under anoxic conditions, the degradation of organic phosphorus saturates the phosphorus element in the water body, thereby inhibiting the decomposition of biological phosphorus. At this time, biological phosphorus can well indicate the change of productivity. The MES shales deposited at a stratified water (Chen et al., 2021), which may have great effect on the enrichments of TOC and phosphorus. Sediment bulk accumulation rates is another major factor influencing the accumulation of phosphorus. Organic carbon accumulation rates show a strong correlation with sediment bulk accumulation rate (Müller and Suess, 1979), although the nature of the relationship differs between fully oxic and fully anoxic environments (Tyson, 2005). In oxic environments, higher sediment bulk accumulation rates minimizes the exposure time of organic matter to aerobic decay in the shallow burial zone (Iversen and Ploug, 2010). Ingall and Van Cappellen (1990) observed that TOC/ P ratios vary in a manner as a function of sedimentation rate. The underlying control on this pattern possibly related to the interplay of sedimentation rates with redox conditions. High TOC:P ratios are



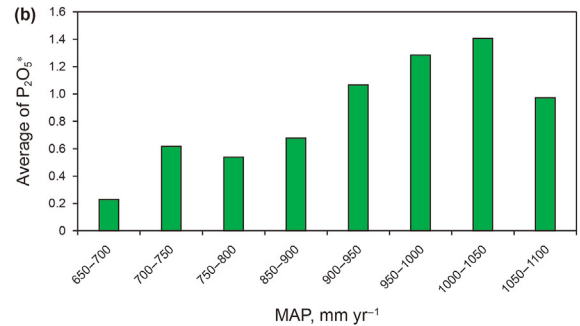
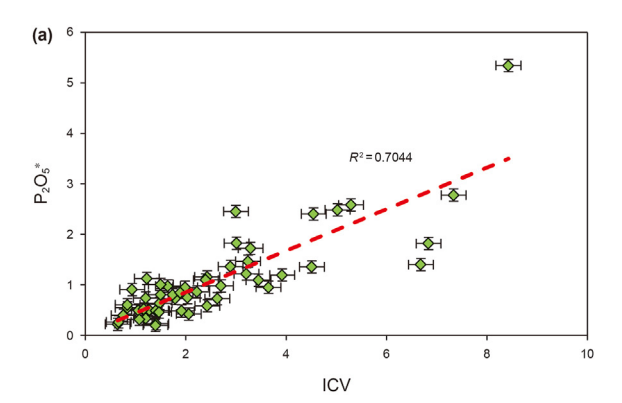


Fig. 13. Shows the variation of the average P₂O₅* along with the intervals of MAT (a) and MAP (b) for the MES shales, respectively.



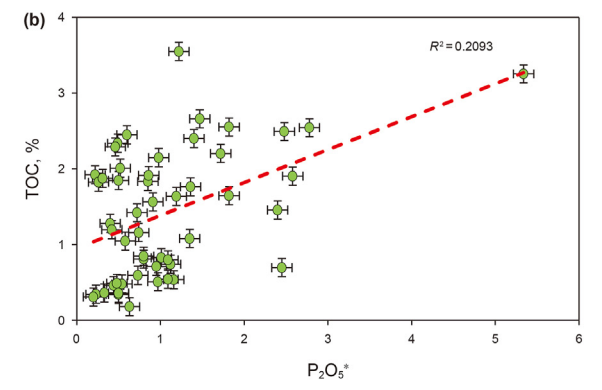


Fig. 14. (a) Shows a positive relation of $P_2O_5^*$ and ICV, and weakly positive relation between TOC and $P_2O_5^*$.

associated with reducing environments (Algeo and Ingall, 2007), which tend to have sedimentation rates between those of highly oxidizing environments in open-ocean settings (low sediment bulk accumulation rates) and those in continent-margin systems (high sediment bulk accumulation rates) (Ingall and Van Cappellen, 1990; Tromp et al., 1995). The MES shales interceded some sandy bands (Fig. 2; Chen et al., 2019), which reflect the change of lithofacies and terrigenous inputs. These lithofacies change show unstable deposition rate of MES shales, thus affecting the accumulation efficiency of TOC and phosphorus.

5.3. Evolution of paleoclimate and chemical weathering

Stratigraphic variations in the values of paleoweathering and paleoclimate proxies are shown in Fig. 15. To more accurately reflect the variation of the weathering conditions during the middle Eocene, the CIA values of the MES shale samples with ICV values less than 1 have been eliminated (Fig. 15). Generally, the variations of CIA, W, MAP and MAT show common trends in which the value decreases from the bottom to top. The decreasing CIA is similar to the previous study in the Dongying Sag (Ma, 2017), supporting the climate transition during MECO epoch. The comparison of CIA changes in the Xining Basin and Qaidam Basin in the same period shows that the East Asian monsoon climate has existed in the middle Eocene period. The MAP decreased along with climate cooling, which resulted in a relatively arid climate that promoted evaporite formation during Eocene. These results may account for the occurrences of carbonate and anhydrite in MES shales (Fig. 4b). This conclusion is consistent with the work of many researchers who have demonstrating that China featured an extensive arid climate at the beginning of the middle Eocene (Meng et al., 2012; Li et al., 2015b; Hou et al., 2017; He et al., 2017; Song et al., 2018; Chen et al., 2018; Wu et al., 2018).

The relatively consistently high CIA, MAP and MAT values throughout the entire succession are abruptly interrupted by low values that corresponding to breaks in the lithological section, with low ICV values (Fig. 15). According to the variations in these proxies, the MES shales could be divided into two stages. The Mann-Whitney U test shows that the two sets of data have statistically significant differences except ICV and P₂O₅*, and the *p*-value were less than 0.05 (Fig. 15). In stage I, the MES shales experienced a relatively gentle climate and moderate chemical weathering, with consistently decreasing trends for CIA, MAP and MAT. This consistently decreasing trends has been also observed in the Dongying and Dongpu Sags (Jiang et al., 2021; Zhu et al., 2022), contrary to the changes in the Xining Basin and Qaidam Basin. It reflects the East Asian monsoon leading to significant difference among the western and eastern China. This change may related to the continuous uplift of the Qinghai Tibet Plateau during this period. The uplifted Qinghai Tibet Plateau blocks the sea breeze from the ancient Talimu Sea in the west and the warm and humid air in the southern Indian Ocean, which lead to the relatively dry climate in the eastern Asian (Bosboom et al., 2011; Carrapa et al., 2015). In this stage, the average MAT was 11.90 °C, the average MAP was 997.92 mm/yr, and the nutrient-rich lakes featured relatively high primary productivity, with an average P₂O₅* value of 1.26. Tectonic activity was relatively high during stage I, with high mean ICV value of 3.02. The MES shales in stage I have low degree of compositional maturity with low average SiO₂/Al₂O₃ value of 3.88. The climate in stage II was cooler and drier than that in stage I, with an average MAT of 10.22 °C and an average MAP of 854.78 mm/yr. This climate also induced relatively high salinity as shown in Fig. 4b, and resulted in weak chemical weathering with relatively low CIA value. The CIA values change shows obvious fluctuation, which also presented in the Dongying sag. This fluctuation hints that there are other factors affecting the sedimentary process, such as tectonic activity. In this

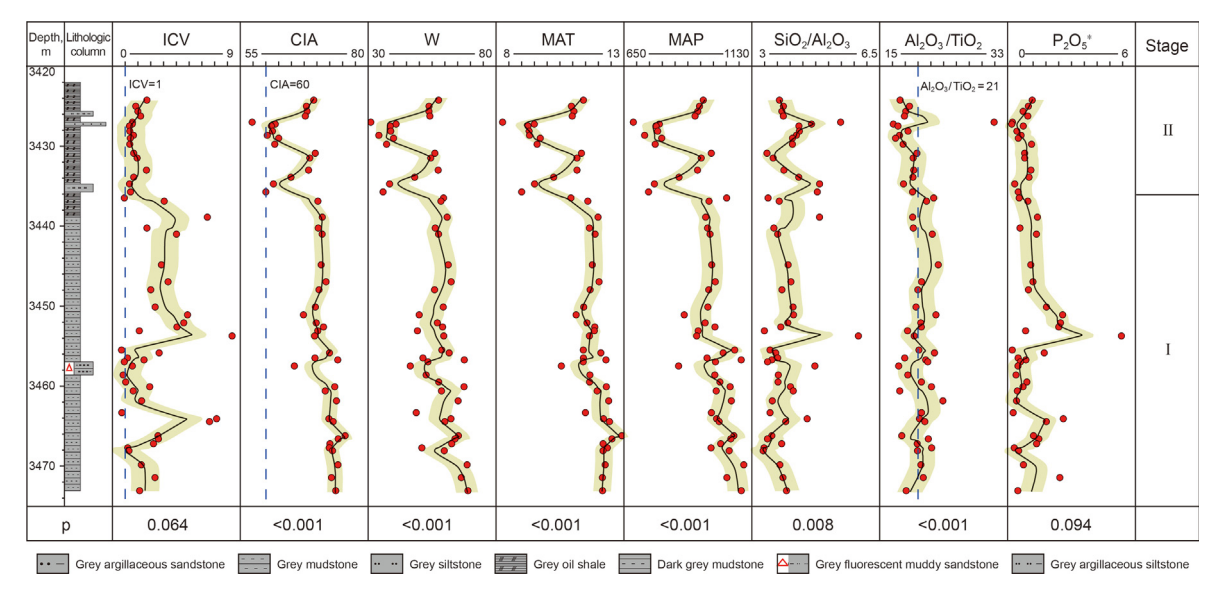


Fig. 15. Stratigraphic variations in the degree of paleoweathering and paleoclimate in the studied section, as measured using geochemical indices. ICV = index of compositional variability; CIA = chemical index of alteration; W = W index; MAT = mean annual temperature; MAP = mean annual precipitation. p is the p-value by Mann-Whitney U test. Kelly shadings prediction intervals at $\alpha = 0.05$ level. The black smoothing trendline is derived by using Locally Weighted Scatterplot Smoothing algorithm.

stage, the structure was relatively stable, with low mean ICV of 1.64. The sediment maturities in this stage were relatively high, with an average SiO_2/Al_2O_3 value of 4.13. The paleolake fertility in this stage was lower than that in stage I. This result suggests that more terrigenous detritus was input into the paleolake from a mixed provenance in stage I. The relatively active tectonics of the first stage may have led to more provenance inputs.

5.4. Periodicity of paleoclimate and chemical weathering

The investigation of the periodicity of the paleoclimate variation in the middle Eocene is valuable and important for understanding the evolution of the global paleoclimate. Four proxies, namely, corrected CIA, MAP, MAT and P₂O₅*, were chosen to determine the periodicity in the paleoenvironment using the wavelet transform technique, and the results are shown in Fig. 16. Three periodic oscillations were revealed in the CIA variation by wavelet transform (Fig. 16), namely, 13.94, 5.38, 0.13 m/cycle. The MAP variation contains five periodic oscillations (13.88, 5.25, 2.63, 1.31, 0.13 m/ cycle), which are similar to those of MAT (13.94, 5.25, 2.25, 0.56, 0.13 m/cycle) and $P_2O_5^*$ (13.94, 5.25, 2.25, 0.56, 0.13 m/cycle). Furthermore, the main periodicity ratios of these proxies are nearly identical, with 1:0.39:0.01 for CIA, 1:0.38:0.19 for MAP, and 1:0.38:0.16 for MAT and $P_2O_5^*$ (Fig. 16). These ratios are indicative of a combination of astronomical periods over the last approximately 50 Ma estimated by Berger et al. (1992), including the short eccentricity cycle (100 k.y.), the obliquity cycle (39 k.y.) and the precession cycle (19 k.y. or 17 k.y.). The MES shale was deposited at approximately 42 Ma, which is close to the estimated time of these astronomical periods. This compelling evidence shows good correspondence between the sedimentary rhythm and orbital forcing, which implies that the variations in chemical weathering and paleoclimate during the middle Eocene were controlled by astronomical periodic oscillation in the form of Milankovitch cycles.

Although the CIA frequencies of 13.94 m/cycle and 5.38 m/cycle are perfectly consistent with the short eccentricity cycle (100 k.y.) and obliquity cycle (39 k.y.), the main frequency ratio of 1:0.39:0.01 implies the absence of a precession cycle. The precession of Earth's rotation axis determines the timing and location of the seasons

with respect to Earth's orbit and drives the climate of Earth (Paillard, 2010). There are two explanation for this situation: (1) insufficient consideration is given to the effect of K-metasomatism on the composition of the MES shale, potentially leading to error in the ICV and CIA, and (2) the calculation of CaO* in section 4.3 is not sufficiently accurate because of the lack of the mineral composition of the MES shale.

The main periodicities of the paleoweathering and paleoclimate indices corresponding to the astronomical periods are shown in Fig. 16. In the MES shale core, the CIA time series contains 3 short eccentricity cycles (100 k.y. and 13.94 m/cycle) and 7 obliquity cycles (39 k.y. and 5.38 m/cycle). The MAP curve contains 3 short eccentricity cycles (100 k.y. and 13.88 m/cycle), 7 obliquity cycles (39 k.y. and 5.25 m/cycle) and 15 precession cycles (19 k.y. and 2.63 m/cycle). The MAT and P₂O₅* curves contain the same numbers of astronomical periods, namely, 3 short eccentricity cycles (100 k.y. and 13.94 m/cycle), 7 obliquity cycles (39 k.y. and 5.25 m/cycle) and 16 precession cycles (17 k.y. and 2.25 m/cycle). Furthermore, an accumulation rate of 0.14 m/ k.y. is calculated according to the analysis above, and this value may correspond to the element accumulation rate or deposition rate. Furthermore, the MAP and MAT curves contain approximately 2.1 short eccentricity cycles and 5.4 obliquity cycles in stage I, and the MAT and MAP decrease from 12.16 °C to 11.59 °C and from 1090.56 mm to 956.68 mm, respectively; therefore, the cooling and drying rates in stage II are 0.27×10^{-2} °C/k.y. and 0.64 mm/k.y., respectively. Because the MAP and MAT deceasing trends were relatively consistent in stage II and represent the trend of the overall climate during deposition of the MES shale, the climatic cooling and drying rates in the midlatitude Bohai Bay Basin during the middle Eocene are estimated to have been 0.27×10^{-2} °C/k.y. and 0.64 mm/k.y., respectively.

In addition, the amplitude of the obliquity cycle in the paleoclimate proxies shown in Fig. 16 is heterogeneous. The amplitudes of the obliquity cycle are weak in stage I and may be disturbed by other superimposed signals, such as those of tectonic activity. However, the amplitudes are stronger in stage II, in which the stable tectonics produced less interference with the astronomically driven climate signals. Therefore, the paleoclimate variation and chemical D. Chen, F.-J. Jiang, X.-Q. Pang et al. Petroleum Science 20 (2023) 1471–1487

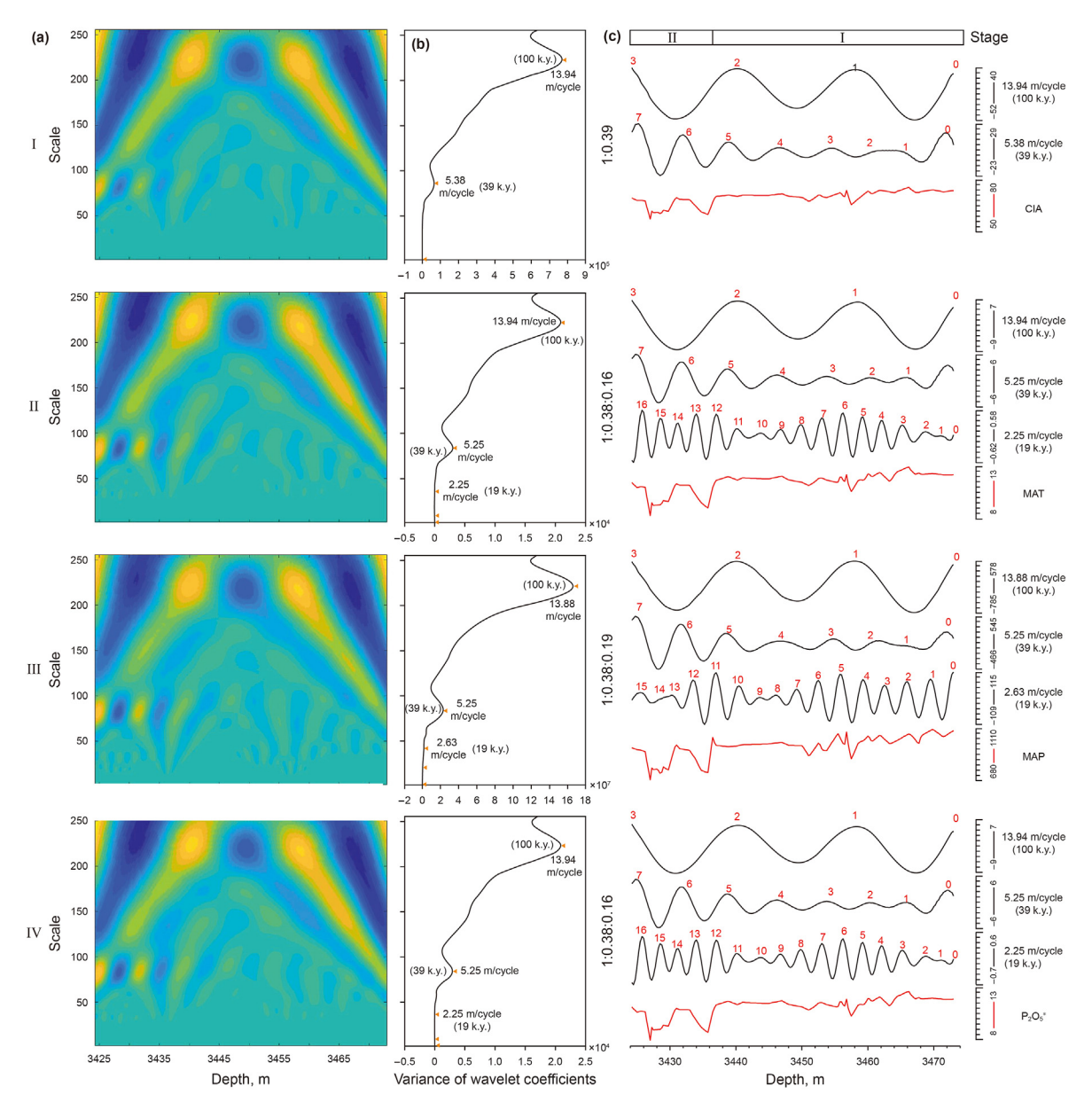


Fig. 16. The results of wavelet analysis for the variation in the CIA (I), MAP (III) and P₂O₅* (IV) during the middle Eocene for the *MES shale*. Wavelet scalograms (a) shows the energy fluctuation with depth at different scales, indicating the different oscillation cycles. (b) show the variograms of real wavelet coefficients, and the extreme points (orange triangle) represent the main frequencies. (c) shows the cycle counting of the main astronomical period.

weathering conditions during the middle Eocene were controlled by the astronomical oscillation cycles and by the tectonic activity in the midlatitude Bohai Bay Basin. The spectral analysis of the proxies revealed cyclicity in the paleoweathering and paleoclimate conditions in the Bohai Bay Basin during the middle Eocene, and these findings can enhance the understanding of global paleoenvironment variation in midlatitude regions during the middle Eocene.

6. Conclusions

Based on major element analysis, this study reveals the middle Eocene terrestrial paleoweathering features and constructed the paleoclimatic evolution profile for the Bohai Bay Basin at Asian in Asia Continent. The Midlatitude Bohai Bay Basin experienced a subtropical monsoon paleoclimate with MAT of 8.3–12.9 °C and

MAP of 685—1100 mm/yr during middle Eocene. The nutrient-rich environment of ancient lake deposited a large number of organic rich *MES shales*. The major element analysis revealed enrichment of calcium and depletion of sodium in the *MES shales* compared to the UCC. The CIA values for the *MES shales* are higher than those of the UCC but similar to those of the PAAS. The *MES shales* experienced moderate paleoweathering with little K-metasomatism. The *MES shales* have a mixed provenance of intermediate igneous rocks with low compositional maturity. According to the climatic variation, the deposition process of the *MES shales* is divided into two stages. In stage I, the paleolake was nutrient rich, and the *MES shales* suffered high chemical weathering due to a warmer and more humid climate. The climate in stage II was entirety cold and dry, and the tectonic activity is relatively stable, facilitating the deposition of *MES shales* with relatively high composition maturity.

Acknowledgment

The research data could be found at https://doi.org/10.5061/ dryad,2547d7wpc. This work was funded by Science Foundation of China University of Petroleum, Beijing (No. 2462022XKBH005), and China Postdoctoral Science Foundation (2022M723487), and the National Science and Technology Major Project of the Ministry of Science and Technology of China (2016ZX05006-006), and PetroChina Project (2021DJ0704). In the process of this research, Jidong Oilfield, China National Petroleum Corporation (CNPC), provided considerable help during the sampling and experiments and provided the basic study data, and we wish to express our gratitude for this assistance. We apologize for the hundreds of papers we were aware of but could not cite. In addition, we are grateful for the help from Boming Zhang and Xiao Liu of PetroChina Jidong Oilfield. We also thank Professor Matthew Steele-MacInnis, Department of Earth & Atmospheric Sciences of University of Alberta, and Doctor Kun Zhang in University College London, and Youwei Wang in Delft University of Technology for their suggestions.

References

- Algeo, T.J., Ingall, E., 2007. Sedimentary Corg: P ratios, paleocean ventilation, and Phanerozoic atmospheric pO₂. Palaeogeogr. Palaeoclimatol. Palaeoecol. 256 (3–4), 130–155. https://doi.org/10.1016/j.palaeo.2007.02.029.
- Allen, M.B., Macdonald, D.I.M., Zhao, X., et al., 1997. Early Cenozoic two-phase extension and late Cenozoic thermal subsidence and inversion of the Bohai Basin, northern China. Mar. Petrol. Geol. 14 (7–8), 951–972. https://doi.org/10.1016/S0264-8172(97)00027-5.
- Ao, H., Dupont-Nivet, G., Rohling, E.J., et al., 2020. Orbital climate variability on the northeastern Tibetan Plateau across the Eocene—Oligocene transition. Nat. Commun. 11, 5249. https://doi.org/10.1038/s41467-020-18824-8.
- Armstrong-Altrin, J.S., Verma, S.P., 2005. Critical evaluation of six tectonic setting discrimination diagrams using geochemical data of Neogene sediments from known tectonic settings. Sediment. Geol. 177 (1–2), 115–129. https://doi.org/ 10.1016/j.sedgeo.2005.02.004.
- Armstrong-Altrin, J.S., Nagarajan, R., Madhavaraju, J., et al., 2013. Geochemistry of the Jurassic and upper cretaceous shales from the Molango region, Hidalgo, eastern Mexico: implications for source-area weathering, provenance, and tectonic setting. C.R. Geosci. 345 (4), 185–202. https://doi.org/10.1016/ j.crte.2013.03.004.
- Awasthi, N., 2017. Provenance and paleo-weathering of Tertiary accretionary prismforearc sedimentary deposits of the Andaman Archipelago, India. J. Asian Earth Sci. 150, 45–62. https://doi.org/10.1016/j.jseaes.2017.10.005.
- Babeesh, C., Achyuthan, H., Jaiswal, M.K., et al., 2017. Late Quaternary loess-like paleosols and pedocomplexes, geochemistry, provenance and source area weathering, Manasbal, Kashmir Valley, India. Geomorphology 284, 191–205. https://doi.org/10.1016/j.geomorph.2017.01.004.
- Bains, S., Corfield, R.M., Norris, R.D., 1999. Mechanisms of climate warming at the end of the Paleocene. Science 285 (5428), 724–727. https://doi.org/10.1126/ science.285.5428.7.
- Bakkiaraj, D., Nagendra, R., Nagarajan, R., et al., 2010. Geochemistry of sandstones from the upper cretaceous Sillakkudi formation, cauvery Basin, southern India: implication for provenance. J. Geol. Soc. India 76, 453–467. https://doi.org/ 10.1007/s12594-010-0128-3.
- Berger, A., Loutre, M.F., Laskar, J., 1992. Stability of the astronomical frequencies over the Earth's history for paleoclimate studies. Science 255 (5044), 560–566. https://doi.org/10.1126/science.255.5044.560.
- Bhatia, M.R., 1983. Plate tectonics and geochemical composition of sandstones. J. Geol. 91 (6), 611–627. https://doi.org/10.1086/628815.
- Bohaty, SM, Zachos, JC, 2003. Significant Southern Ocean warming event in the late middle Eocene. Geology 31 (11), 1017–1020.
- Bohaty, SM, Zachos, JC, Florindo, F, et al., 2009. Coupled greenhouse warming and deep-sea acidification in the middle Eocene. Paleoceanography 24 (2).
- Bosboom, R.E., Dupont-Nivet, G., Houben, A.J.P., et al., 2011. Late Eocene sea retreat from the Tarim Basin (West China) and concomitant Asian paleoenvironmental change. Palaeogeogr. Palaeoclimatol. Palaeoecol. 299 (3/4), 385–398. https://doi.org/10.1016/j.palaeo.2010.11.019.
- Bock, B., McLennan, S.M., Hanson, G.N., 1998. Geochemistry and provenance of the middle ordovician Austin glen member (Normanskill formation) and the Taconian orogeny in New England. Sedimentology 45, 635–655. https://doi.org/10.1046/j.1365-3091.1998.00168.x.
- Canfield, D.E., 1994. Factors influencing organic carbon preservation in marine sediments. Chem. Geol. 114 (3–4), 315–329. https://doi.org/10.1016/0009-2541(94)90061-2.
- Carrapa, B., DeCelles, P.G., Wang, X., et al., 2015. Tectono-climatic implications of Eocene paratethys regression in the Tajik Basin of central Asia. Earth Planet Sci.

- Lett. 424, 168-178. https://doi.org/10.1016/j.epsl.2015.05.034.
- Chen, D., Pang, X., Wang, Y., et al., 2019. Palaeoenvironmental periodisms of middle Eocene terrestrial sediments in Bohai Bay Basin, eastern China, and their implications for organic matter accumulation. Mar. Petrol. Geol. 104060. https://doi.org/10.1016/j.marpetgeo.2019.104060.
- Chen, D., Pang, X., Li, L., et al., 2021. Organic geochemical characteristics and shale oil potential of the middle Eocene early-mature shale in the Nanpu Sag, Bohai Bay Basin, Eastern China. Mar. Petrol. Geol. 133, 105248. https://doi.org/10.1016/j.marpetgeo.2021.105248.
- Chen, J., Zhang, S., Sun, S., et al., 2006. Main factors influencing marine carbonate source rock formation. Acta Geolo Gica Sinica 80 (3), 467–471.
- Chen, Z., Li, M., Ma, X., et al., 2018. Generation kinetics based method for correcting effects of migrated oil on Rock-Eval data-An example from the Eocene Qianjiang Formation, Jianghan Basin, China. Int. J. Coal Geol. 195, 84–101. https://doi.org/10.1016/j.coal.2018.05.010.
- Chung, S.L., Lo, C.H., Lee, T.Y., et al., 1998. Diachronous uplift of the Tibetan plateau starting 40? Myr ago. Nature 394 (6695), 769–773. https://doi.org/10.1038/29511.
- Condie, K.C., 1993. Chemical composition and evolution of the upper continental crust: contrasting results from surface samples and shales. Chem. Geol. 104, 1–37. https://doi.org/10.1016/0009-2541(93)90140-E.
- Cox, R., Lowe, D.R., Cullers, R.L., 1995. The influence of sediment recycling and basement composition of evolution of mudrock chemistry in the southwestern United States. Geochem. Cosmochim. Acta 59, 19–40. https://doi.org/10.1016/0016-7037(95)00185-9.
- Cullers, R.L., 2000. The geochemistry of shales, siltstones and sandstones of Penn-sylvanian permian age, Colorado, USA: implications for provenance and metamorphic studies. Lithos 51, 181–203. https://doi.org/10.1016/S0024-4937(99)00063-8.
- Cullers, R.L., 2002. Implications of elemental concentrations for provenance, redox conditions, and metamorphic studies of shales and limestones near Pueblo, CO, USA. Chem. Geol. 191, 305–327. https://doi.org/10.1016/S0009-2541(02)00133-
- Dong, Y., Xiao, L., Zhou, H., et al., 2010. The Tertiary evolution of the prolific Nanpu sag of Bohai Bay Basin, China: constraints from volcanic records and tectonostratigraphic sequences. GSA Bull 122 (3–4), 609–626. https://doi.org/10.1130/B30041.1.
- Eberl, D.D., Farmer, V.C., Barrer, R.M., 1984. Clay mineral formation and transformation in rocks and soils. Phil. Trans. Roy. Soc. Lond. 311, 41–57. https://doi.org/10.1098/rsta.1984.0026.
- Fadipe, O.A., Carey, P.F., Akinlua, A., et al., 2011. Provenance, diagenesis and reservoir quality of the lower cretaceous sandstone of the Orange Basin, South Africa. S. Afr. J. Geol. 114 (3–4), 433–448. https://doi.org/10.2113/gssajg.114.3-4.433.
- Fatima, S., Khan, M.S., 2012. Petrographic and geochemical characteristics of Mesoproterozoic Kumbalgarh clastic rocks, NW Indian shield: implications for provenance, tectonic setting, and crustal evolution. Int. Geol. Rev. 54 (10), 1113–1144. https://doi.org/10.1080/00206814.2011.623032.
- Fedo, C.M., Nesbitt, H.W., Young, G.M., 1995. Unraveling the effects of potassium metasomatism in sedimentary rocks and paleosols, with implications for paleoweathering conditions and provenance. Geology 23, 921–924. https://doi.org/10.1130/0091-7613(1995)023<0921:UTEOPM>2.3.CO;2.
- Fedo, C.M., Eriksson, K.A., Krogstad, E.J., 1996. Geochemistry of shales from the Archean (-3.0 Ga) Buhwa Greenstone Belt. Zimbabwe: implications for provenance and source area weathering. Geochem. Cosmochim. Acta 60, 1751–1763. https://doi.org/10.1016/0016-7037(96)00058-0.
- Gabbott, S.H., 1998. Taphonomy of the Ordovician Soom Shale Lagerstatte: an example of soft tissue preservation in clay minerals. Palaeontology 41, 631–667.
- Guo, Y., Pang, X., Dong, Y., et al., 2013. Hydrocarbon generation and migration in the Nanpu Sag, Bohai Bay Basin, eastern China: insight from basin and petroleum system modeling. India. J. Asian Earth Sci. 77, 140—150. https://doi.org/10.1016/j.jseaes.2013.08.033.
- Hao, Q., Guo, Z., Qiao, Y., et al., 2010. Geochemical evidence for the provenance of middle Pleistocene loess deposits insouthern China. Quat. Sci. Rev. 29 (23), 3317–3326. https://doi.org/10.1016/j.quascirev.2010.08.004.
- Hayashi, K.I., Fujisawa, H., Holland, H.D., et al., 1997. Geochemistry of ~1.9 Ga sedimentary rocks from Northeastern labrador, Canada. Geochem. Cosmochim. Acta 61, 4115–4137. https://doi.org/10.1016/S0016-7037(97)00214-7.
- He, J., Ding, W., Jiang, Z., et al., 2017. Mineralogical and chemical distribution of the Es₃, oil shale in the Jiyang Depression, Bohai Bay Basin (E China): implications for paleoenvironmental reconstruction and organic matter accumulation. Mar. Petrol. Geol. 81, 196–219. https://doi.org/10.1016/j.marpetgeo.2017.01.007.
- Hecky, R.E., Kilham, P., 1988. Nutrient limitation of phytoplankton in freshwater and marine environments: review of recent evidence on the effects of enrichment. Limnol. Oceanogr. 33, 796–822. https://doi.org/10.4319/lo.1988.33.4part2.0796.
- Herron, M.M., 1988. Geochemical classification of terrigenous sands and shales from core or log data. J. Sediment. Res. 58 (5), 820–829. https://doi.org/10.1306/212F8E77-2B24-11D7-8648000102C1865D.
- Hou, Y., Wang, F., He, S., et al., 2017. Properties and shale oil potential of saline lacustrine shales in the Qianjiang Depression, Jianghan Basin, China. Mar. Petrol. Geol. 86, 1173–1190. https://doi.org/10.1016/j.marpetgeo.2017.07.008.
- Howarth, R.W., Marino, R., Cole, J.J., 1988. Nitrogen fixation in freshwater, estuarine and marine ecosystMES. 2. Biogeochemical controls. Limnol. Oceanogr. 33, 688–701. https://doi.org/10.4319/lo.1988.33.4part2.0688.
- Ingall, E.D., Van Cappellen, P., 1990. Relation between sedimentation rate and burial of organic phosphorus and organic carbon in marine sediments. Geochem.

- Cosmochim. Acta 54 (2), 373–386. https://doi.org/10.1016/0016-7037(90)
- Iversen, M.H., Ploug, H., 2010. Ballast minerals and the sinking carbon flux in the ocean: carbon-specific respiration rates and sinking velocity of marine snow aggregates. Biogeosciences 7 (9), 2613–2624. https://doi.org/10.5194/bg-7-2613-2010.
- Jahren, A.H., Arens, N.C., Sarmiento, G., et al., 2001. Terrestrial record of methane hydrate dissociation in the Early Cretaceous. Geology 29 (2), 159–162. https:// doi.org/10.1130/0091-7613(2001)029<0159:TROMHD>2.0.CO;2.
- Jiang, H., Wang, H., Lin, Z., et al., 2009. Periodic rifting activity and its controlling on sedimentary filling of Paleogene period in Nanpu sag. Acta Sedmentologica Sinica 27 (5), 976–982. https://doi.org/10.1016/S1874-8651(10)60080-4.
- Jiang, F.J., Pang, X.Q., Bai, J., et al., 2016. Comprehensive assessment of source rocks in the Bohai Sea area, eastern China. AAPG Bull. 100 (6), 969–1002. https:// doi.org/10.1306/02101613092.
- Jiang, F.J., Chen, D., Zhu, C.X., et al., 2021. Mechanisms for the anisotropic enrichment of organic matter in saline lake basin: a case study of the Early Eocene Dongpu Depression, eastern China. J. Petrol. Sci. Eng. https://doi.org/10.1016/i.petrol.2021.110035.
- Kargaranbafghi, F, Neubauer, F, 2017. Tectonic forcing to global cooling and aridification at the Eocene-Oligocene transition in the Iranian plateau[J]. Global and planetary change 171, 248–254.
- Khudoley, A.K., Rainbird, R.H., Stern, R.A., et al., 2001. Sedimentary evolution of the Riphean-Vendian basin of southwestern Siberia. Precambrian Res. 111, 129–163. https://doi.org/10.1016/S0301-9268(01)00159-0
- https://doi.org/10.1016/S0301-9268(01)00159-0.
 Li, W., Lu, S., Xue, H., Zhang, P., et al., 2015. The formation environment and developmental models of argillaceous dolomite in the Xingouzui Formation, the Jianghan Basin. Mar. Petrol. Geol. 67, 692–700. https://doi.org/10.1016/j.marpetgeo.2015.06.011.
- Lei, H.R., Jiang, Z.X., Zhou, H.K., 2018. Analysis of paleoclimate evolution of the hyperthermal period in the early Paleogene: taking the Dongying depression as an example. Earth Sci. Front. 25 (4), 176–184. https://doi.org/10.13745/ j.esf.yx.2017-10-2.
- Ma, Y., 2017. Lacustrine Shale Stratigraphy and Eocene Climate Recorded in the Jiyang Depression in East China. Doctoral Thesis of China University of Geosciences.
- Maynard, J.B., 1992. Chemistry of modern soils as a guide to interpreting Precambrian paleosols. J. Geol. 100, 279–289. https://doi.org/10.1086/629632.
- McInerney, F.A., Wing, S.L., 2011. The Paleocene-Eocene Thermal Maximum: a perturbation of carbon cycle, climate, and biosphere with implications for the future. Annu. Rev. Earth Planet Sci. https://doi.org/10.1146/annurev-earth-040610-133431.
- McLennan, S.M., 1993. Weathering and global denudation. J. Geol. 101 (2), 295–303. https://doi.org/10.1086/648222.
- Meng, Q., Liu, Z., Bruch, A.A., Liu, R., et al., 2012. Palaeoclimatic evolution during Eocene and its influence on oil shale mineralisation, Fushun basin, China. J. Asian Earth Sci. 45, 95–105. https://doi.org/10.1016/j.jseaes.2011.09.021.
- Miller, K.G., Wright, J.D., Fairbanks, R.G., 1991. Unlocking the ice house: Oligocene-Miocene oxygen isotopes, eustasy, and margin erosion. J. Geophys. Res. Solid Earth 96 (B4), 6829–6848. https://doi.org/10.1029/90JB02015@10.1002/(ISSN) 2169–9356.LTSLC1.
- Müller, P.J., Suess, E., 1979. Productivity, sedimentation rate, and sedimentary organic matter in the ocean—I. Organic carbon preservation. Deep-Sea Res. 26, 1347–1362. https://doi.org/10.1016/0198-0149(79)90003-7.
- Muhs, D.R., Bettis, E.A., Been, J., et al., 2001. Impact of climate and parent material on chemical weathering in loess-derived soils of the Mississippi river valley. Soil Sci. Soc. Am. J. 65, 1761–1777. https://doi.org/10.2136/sssaj2001.1761.
- Nesbitt, H.W., Young, G.M., 1982. Early Proterozoic climates and plate motions inferred from major element chemistry of lutites. Nature 299 (5885), 715. https://doi.org/10.1038/299715a0.
- Nesbitt, H.W., Young, G.M., 1984. Prediction of some weathering trends of plutonic and volcanic rocks based on thermodynamic and kinetic considerations. Geochem. Cosmochim. Acta 48 (7), 1523–1534. https://doi.org/10.1016/0016-7037(84)90408-3
- Nesbitt, H.W., Young, G.M., 1989. Formation and diagenesis of weathering profiles. J. Geol. 97 (2), 129–147. https://doi.org/10.1086/629290.
- Nesbitt, H.W., Young, G.M., McLennan, S.M., et al., 1996. Effects of chemical weathering and sorting on the petrogenesis of siliciclastic sediments, with implications for provenance studies. J. Geol. 104 (5), 525–542. https://doi.org/10.1086/629850.
- Ohta, T., 2004. Geochemistry of Jurassic to earliest Cretaceous deposits in the Nagato Baisn, SW Japan: implication of factor analysis to sorting effects and provenance signatures. Sediment. Geol. 171, 159–180. https://doi.org/10.1016/i.sedgeo.2004.05.014.
- Ohta, T., Arai, H., 2007. Statistical empirical index of chemical weathering in igneous rocks: a new tool for evaluating the degree of weathering. Chem. Geol. 240 (3–4), 280–297. https://doi.org/10.1016/j.chemgeo.2007.02.017.
- Ohta, T., Li, G., Hirano, H., et al., 2011. Early Cretaceous terrestrial weathering in Northern China: relationship between paleoclimate change and the phased evolution of the Jehol Biota. J. Geol. 119 (1), 81–96. https://doi.org/10.1086/657341.
- Paillard, D., 2010. Climate and the orbital parameters of the Earth. C.R. Geosci. 342 (4–5), 273–285. https://doi.org/10.1016/j.crte.2009.12.006.
- Panahi, A., Young, G.M., Rainbird, R.H., 2000. Behavior of major and trace elements (including REE) during Paleoproterozoic pedogenesis and diagenetic alteration

- of an Archean granite near Ville Marie, Quebec, Canada. Geochem. Cosmochim. Acta 64 (13), 2199–2220. https://doi.org/10.1016/S0016-7037(99)00420-2.
- Panchuk, K., Ridgwell, A., Kump, L.R., 2008. Sedimentary response to Paleocene-Eocene Thermal Maximum carbon release: a model-data comparison. Geology 36, 315–318. https://doi.org/10.1130/G24474A.1.
- Passchier, S., Bohaty, S.M., Jiménez-Espejo, F., et al., 2013. Early Eocene to middle Miocene cooling and aridification of East Antarctica. Geochem. Geophy Geosy. 14 (5), 1399–1410. https://doi.org/10.1002/ggge.20106.
- Passchier, S., Ciarletta, D.J., Miriagos, T.E., et al., 2017. An Antarctic stratigraphic record of stepwise ice growth through the Eocene-Oligocene transition. GSA Bull 129 (3–4). 318–330. https://doi.org/10.1130/B31482.1.
- Perri, F., Critelli, S., Dominici, R., et al., 2012. Provenance and accommodation pathways of late Quaternary sediments in the deepwaternorthern Ionian Basin. southern Italy. Sediment Geol. 280, 44–59. https://doi.org/10.1016/j.sedgeo.2012.01.007.
- Perri, F, Dominici, R, Pera, EL, et al., 2016. Holocene sediments of the Messina Strait (southern Italy): relationships between source area and depositional basin. Mar Petrol Geol 77, 55–66. https://doi.org/10.1016/j.marpetgeo.2016.07.010.
- Perri, F., Ohta, T., 2014. Paleoclimatic conditions and paleoweathering processes on Mesozoic continental redbeds from Western-central Mediterranean Alpine chains. Palaeogeogr. Palaeoclimatol. Palaeoecol. 395, 44–57. https://doi.org/ 10.1016/j.palaeo.2013.12.029.
- Perri, F., 2018. Reconstructing chemical weathering during the Lower Mesozoic in the Western-Central Mediterranean area: a review of geochemical proxies. Geol. Mag. 155 (4), 944–954. https://doi.org/10.1017/S0016756816001205.
- Phipps, D., Playford, G., 1984. Laboratory Techniques for Extraction of Palynomorphs from Sediments.
- Potter, P.E., 1978. Petrology and chemistry of modern big river sands. J. Geol. 86, 423–449. https://doi.org/10.1086/649711.
- Prothero, D.R., 2009. Paleogene climates. Encyclopedia of Paleoclimatology and Ancient Environments 728–733. https://doi.org/10.1007/978-1-4020-4411-3_
- Rieu, R., Allen, P.A., Plotze, M., et al., 2007. Climatic cycles during a Neoproterozoic "snowball" glacial epoch. Geology 35 (4), 299–302. https://doi.org/10.1130/G23400A.1
- Rohl, U., Bralower, T.J., Norris, R.D., et al., 2000. New chronology for the late Paleocene thermal maximum and its environmental implications. Geology 28 (10), 927–930. https://doi.org/10.1130/0091-7613(2000)28<927: NCFTLP>2.0.CO:2.
- Roser, B.P., Korsch, R.J., 1986. Determination of tectonic setting of sandstone-mudstone suites using SiO₂ content and K₂O/Na₂O ratio. J. Geol. 94 (5), 635–650. https://doi.org/10.1086/629071.
- Roser, B.P., Korsch, R.J., 1988. Provenance signatures of sandstone-mudstone suites determined using discriminant function analysis of major-element data. Chem. Geol. 67, 119–139. https://doi.org/10.1016/0009-2541(88)90010-1.
- Roser, B.P., Cooper, R.A., Nathan, S., et al., 1996. Reconnaissance sandstone geochemistry, provenance, and tectonic setting of the lower Paleozoic terranes of the West Coast and Nelson, New Zealand. N. Z. J. Geol. Geophys. 39 (1), 1–16. https://doi.org/10.1080/00288306.1996.9514690.
- Schindler, D.W., 1975. Whole-lake eutrophication experiments with phosphorus, nitrogen and carbon. Int. er. Theor. Angew. Limnol. Verh. 19, 3221–3231. https://doi.org/10.1080/03680770.1974.11896436.
- Schmitz, B., Charisi, S.D., Thompson, E.I., et al., 1997. Barium, SiO₂ (excess), and P₂O₅ as proxies of biological productivity in the Middle East during the Palaeocene and the latest Palaeocene benthic extinction event. Terra. Nova 9 (2), 95–99. https://doi.org/10.1111/j.1365-3121.1997.tb00011.x.
- Schoepfer, S.D., Shen, J., Wei, H., et al., 2015. Total organic carbon, organic phosphorus, and biogenic barium fluxes as proxies for paleomarine productivity. Earth Sci. Rev. 149, 23–52. https://doi.org/10.1016/j.earscirev.2014.08.017.
- Sheldon, N.D., Retallack, G.J., Tanaka, S., 2002. Geochemical climofunctions from North American soils and application to paleosols across the Eocene-Oligocene boundary in Oregon. J. Geol. 110 (6), 687–696. https://doi.org/10.1086/342865.
- Sheldon, N.D., Mitchell, R.L., Collinson, M.E., et al., 2009. Eocene-Oligocene Transition Paleoclimatic and Paleoenvironmental Record from the Isle of Wight (UK). The Late Eocene Earth-Hothouse, Icehouse, and Impacts, vol. 452. Geological Society of America Special Paper, pp. 249–259. https://doi.org/10.1130/2009.2452(16.
- Smith, V.H., 1983. Low nitrogen to phosphorus ratios favor dominance by bluegreen algae in lake hytoplankton. Science 221, 669–671. https://doi.org/ 10.1126/science.221.4611.669.
- Song, Z., Liu, G., 1983. Tertiary sporopollen assemblages in Tibet and their palaeogeographic significance. Stratigr. Paleontol. 11, 81–86.
- Song, B., Zhang, K., Zhang, L., et al., 2018. Qaidam Basin paleosols reflect climate and weathering intensity on the northeastern Tibetan Plateau during the early Eocene climatic Optimum. Palaeogeogr. Palaeoclimatol. Palaeoecol. 512, 6–22. https://doi.org/10.1016/j.palaeo.2018.03.027.
- Spears, D.A., Duff, P.M., Caine, P.M., 1988. West warterberg tonstein, South Africa. Int. J. Coal Geol. 9, 221–233. https://doi.org/10.1016/0166-5162(88)90014-6.
- Szymański, W., Szkaradek, M., 2018. Andesite weathering and soil formation in a moderately humid climate: a case study from the Western Carpathians (southern Poland). Carpath. J. Earth Env. 13 (1), 93–105. https://doi.org/10.26471/cjees/2018/013/010.
- Tao, S., Wang, Y., Tang, D., et al., 2012. Organic petrology of fukang permian lucaogou formation oil shales at the northern foot of Bogda mountain, Junggar Basin, China. Int. J. Coal Geol. 99, 27–34. https://doi.org/10.1016/

j.coal.2012.05.001.

- Taylor, S.R., McLennan, S.M., 1985. The Continental Crust: its Composition and Evolution. Blackwell, Oxford. https://doi.org/10.1086/629067.
- Tromp, T.K., Van Cappellen, P., Key, R.M., 1995. A global model for the early diagenesis of organic carbon and organic phosphorus in marine sediments. Geochem. Cosmochim. Acta 59, 1259-1284. https://doi.org/10.1016/0016-7037(95)00042-X.
- Tyson, R.V., 2005. The "productivity versus preservation" controversy; cause, flaws, and resolution, In: Harris, N.B. (Ed.), Deposition of Organic-Carbon-Rich Sediments: Models, Mechanisms, and Consequences, vol. 82. Society for Sedimentary Geology (SEPMSSG) Special Publication, pp. 7–33.
- Újvári, G., Varga, A., Raucsik, B., et al., 2014. The Paks loess-paleosol sequence: a record of chemical weathering and provenance for the last 800 ka in the mid-Quat. Int. 319, 22-37. https://doi.org/10.1016/ Carnathian Basin j.quaint.2012.04.004.
- Wang, W., Chen, G., Chen, Y., et al., 2003. Tertiary palynostratigraphy of the Ningming basin, Guangxi. J. stratigr. 27 (4), 324–327.
 Wang, S., Ding, J., Li, Y., 2005. Application of Wavelet Analysis in Hydrogeology.
- Chemical Industry Press, Beijing, pp. 1–19 (in Chinese).
 Ward, C.R., Corcoran, J.F, Saxby, J.D, et al., 1996. Occurrence of phosphorus minerals in Australian coal seams. Int. J. Coal Geol. 30 (3), 185–210. Wu, L., Wang, F., Wang, D., et al., 2018. The lithologic differences between the third
- and fourth members of the Eocene Shahejie Formation in the Bohai Bay Basin and the associated climatic evolution. Geol. J. 53 (3), 788-802. https://doi.org/ 10.1002/gj.2927.
- Xia, X.F., Zhang, N., Yu, J.X., et al., 2015. Eocene-Oligocene palynology and palynology and biostratigraphic correlation in the Nanpu Sag, Bohai Bay Basin, China. Acta Micropalaeontol. Sin. 32 (3), 269-284.

- Young, G.M., Nesbitt, H.W., 1998. Processes controlling the distribution of Ti and Al in weathering profiles, siliciclastic sediments and sedimentary rocks. J. Sediment. Res. 68 (3), 448-455. https://doi.org/10.2110/jsr.68.448.
- Zachos, JC, Dickens, GR, 2000. An assessment of the biogeochemical feedback response to the climatic and chemical perturbations of the LPTM. Gff 122 (1), 188-189.
- Zachos, J.C., Lohmann, K.C., Walker, J.C.G., et al., 1993. Abrupt climate change and transient climates during the Paleogene: a marine perspective. J. Geol. 101 (2), 191-213. https://doi.org/10.1086/648216.
- Zachos, J.C., Stott, L.D., Lohmann, K.C., 1994. Evolution of early Cenozoic marine temperatures. Paleoceanogr. Paleoclimatol. 9 (2), 353-387. https://doi.org/ 10.1029/93PA03266
- Zachos, J., Pagani, M., Sloan, L., et al., 2001. Trends, rhythms, and aberrations in global climate 65 Ma to present. Science 292 (5517), 686-693. https://doi.org/ 10.1126/science.1059412.
- Zhang, S., Li, B., He, Z., 2016. The imbalance property of ancient salinity in Bohaiwan Basin during E₃₃-E₅₄ stage in the Paleogene. Acta Sedimentol. Sin. 34 (2), 397–403. https://doi.org/10.14027/j.cnki.cjxb.2016.02.018.
- Zhang, T., Yin, F., 2005. Sporopollen assemblage from the Shahejie Formation in the Tanhai area of Huanghua depression. J. Northwest Univ. (Nat. Sci. Ed.) 35 (1),
- Zheng, H.J., Dong, Y.X., Zhu, G.Y., et al., 2007. High-quality source rocks in Nanpu sag. Explor. Dev+. 34 (4), 385-391.
- Zhu, C., Jiang, J., Zhang, P., et al., 2022. Effect of petroelum chemical fraction and residual oil content in saline lacustrine organic-rich shale: a case study from the Paleogene Dongpu depression of North China. Petrol. Sci. https://doi.org/ 10.1016/j.petsci.2022.09.013.